Electrochimica Acta 497 (2024) 144545

Contents lists available at ScienceDirect

Electrochimica Acta

journal homepage: www.journals.elsevier.com/electrochimica-acta

Pourbaix diagrams for iron-chromium alloys in lithium bromide absorption machines

M.J. Muñoz-Portero [a], T. Nachiondo [b], J. García-Antón [a,*]

[a] Ingeniería Electroquímica y Corrosión, Instituto Universitario de Seguridad Industrial, Radiofísica y Medioambiental, Universitat Politècnica de València, Camino de Vera s/n, 46022 Valencia, Spain
[b] Departamento de Informática de Sistemas y Computadores, Universitat Politècnica de València, Camino de Vera s/n, 46022 Valencia, Spain

ARTICLE INFO

Keywords:
Corrosion
Lithium bromide
Passivation
Pourbaix diagram
Stainless steel

ABSTRACT

The influence of lithium bromide concentration on the Pourbaix diagrams for iron-chromium alloys is evaluated in this work, which allows for predicting the corrosion to stainless steels exposed to the aggressive operating conditions of lithium bromide absorption machines (concentrations ranging from: 400–992 g/L). The novelty of this work is found in the development of Pourbaix diagrams for the Fe-Cr-Br^--H_2O quaternary system in aqueous solutions with a high concentration of lithium bromide, a topic which has not yet been studied. Results show that the corrosion region at acid pH corresponding to the aqueous species $FeBr_2$(aq), $FeBr_3$(aq), Cr^{+2}, $CrOH^{+2}$, Cr^{+3} or $CrBr^{+2}$ shifts to higher pHs with increasing lithium bromide concentration, which decreases the immunity region of iron and chromium and decreases the passivation region of the solid species $FeCr_2O_4$, Fe_2O_3 and Cr_2O_3.

1. Introduction

Absorption refrigeration machines are taking on a new importance in various refrigeration applications compared to conventional vapour compression refrigeration systems because the former offer advantages such as reduced electricity consumption, low maintenance costs, and use of refrigerants with a zero contribution to ozone layer depletion and near-zero global warning potential [1-4]. One of the most widely used working fluids in commercial devices is the solution of lithium bromide (LiBr) in water (H_2O), with water being the refrigerant and LiBr the absorbent [5-13]. Although the LiBr/H_2O solution has excellent properties, this working fluid can lead to severe corrosion problems to the metallic materials used inside these devices, such as carbon steel [14-19] and stainless steel [20-26]. In relation to these types of steels, stainless steels present higher corrosion resistance in LiBr/H_2O solutions than carbon steels since stainless steels contain chromium (Cr) in their composition. Cr has great affinity for oxygen and forms a passive layer when it reacts with oxygen, thus preventing corrosion to iron (Fe) [27-28]. However, the high concentrations of LiBr used in the absorption machines can generate pitting corrosion in stainless steels, causing failures in these devices. For this reason, there is a pressing and practical need to predict corrosion in the particular situation of stainless steels exposed to the aggressive environment found inside LiBr absorption machines.

Pourbaix diagrams (Potential vs. pH diagrams) are appropriate for predicting metallic materials' corrosion behaviour in diverse environments. They have applications in the energy industry and the hydrometallurgy field. Pourbaix diagrams represent the thermodynamic equilibria of a metal and its compounds in a specific aqueous medium, delimiting the stability zones of each species. Simplified Pourbaix diagrams indicate the zones of corrosion, immunity, and passivation, rather than stable species. In addition to showing the stability region of a metal (immunity), they also show the stability regions of aqueous compounds (corrosion) and solid compounds (passivation).

Pourbaix diagrams for ferrous materials (iron and its alloys) in H_2O have been developed in previous works [29-39]. The influence of aggressive ions such as carbonates (CO_3^{-2}) and chlorides (Cl^-) on the Pourbaix diagrams for iron and its alloys in H_2O have been reported in several works. For example, Ph. Refait et al. developed the Pourbaix diagram of iron in carbonate-containing media [40-41]. Zhou et al. established the Pourbaix diagram for the iron-chloride-water system applied to supercritical water oxidation technology [42]. Zhao et al. developed the Pourbaix diagram for the iron-chromium-water-chloride-carbon dioxide quinary system in the oilfield environment [43]. Pourbaix diagrams have not been found for stainless steels in aggressive bromide ion (Br^-) presence.

* Corresponding author.
E-mail address: jgarciaa@iqn.upv.es (J. García-Antón).

https://doi.org/10.1016/j.electacta.2024.144545
Received 2 May 2024; Received in revised form 31 May 2024; Accepted 3 June 2024
Available online 6 June 2024

Table 1
Chemical species for the Fe-Cr-Br^--H_2O system.

Species	Oxidation number[a]	State[b]	ΔG_f^o (kJ/mol)	References[c]
H^+		aq	0	49, 50
H_2		g	0	49, 50
O_2		g	0	49, 50
H_2O		l	– 237.178	49, 50
OH^-		aq	– 157.293	49, 50
Fe	0	s	0	29
$Fe(OH)_2$(s)	II	s	– 491.98	29
α-Fe_3O_4	II/III	s	– 1012.57	29
α-Fe_2O_3	III	s	– 744.3	29
Fe^{+2}	II	aq	– 91.88	29
$Fe(OH)_4^{-2}$	II	aq	– 775.87	29
Fe^{+3}	III	aq	– 17.59	29
$Fe(OH)_4^-$	III	aq	– 842.85	29
FeO_4^{-2}	VI	aq	– 322	29
Cr	0	s	0	51
Cr_2O_3	III	s	– 1053.09	51
Cr^{+2}	II	aq	– 174	51
Cr^{+3}	III	aq	– 215	51
$CrOH^{+2}$	III	aq	– 431.8	51
$Cr(OH)_4^-$	III	aq	– 1005.89	51
CrO_4^{-2}	VI	aq	– 727.75	51
$HCrO_4^-$	VI	aq	– 765.14	51
$FeCr_2O_4$	II and III	s	– 1346.0	30
Br^-		aq	– 103.97	49, 50
$FeBr_2$(aq)	II	aq	– 286.81	49, 50
$FeBr_3$(aq)	III	aq	– 316.7	49, 50
$CrBr^{+2}$	III	aq	– 302	49

[a] Oxidation number for the iron and chromium species.
[b] aq = aqueous, g = gas, l = liquid, and s = solid.
[c] Reference from which the ΔG_f^o data are obtained.

This work aims to predict the corrosion risks of stainless steel exposed to the aggressive environment used inside the LiBr absorption machines. Pourbaix diagrams and simplified Pourbaix diagrams are developed for Fe-Cr alloys in aqueous solutions with high concentrations of LiBr (400–992 g/L) to simulate the aggressive conditions in the LiBr absorption machines. The novel contribution of the work comes in its evaluation of the influence of LiBr concentration on the diagrams for the Fe-Cr-Br^--H_2O quaternary system, which has not yet been studied.

2. Materials and methods

The methodology followed in this paper is analogous to that detailed in prior works about the Pourbaix diagrams for pure metals (copper, nickel, chromium, titanium, and iron) exposed to aqueous solutions with high concentrations of LiBr [44-48]. In this work, appropriate adaptations are made for Fe-Cr alloys.

2.1. Chemical species

A total of 21 chemical species from the Fe-Cr-Br^--H_2O quaternary system are considered (7 solid species and 14 aqueous species), as shown in Table 1, which are classified into three types:

1. Species containing iron (11 chemical species):
   - Solid iron species (4 species):
     - Metal: Fe.
     - Fe (II) compounds: $Fe(OH)_2$(s).
     - Fe (III) compounds: α-Fe_2O_3.
     - Fe (II/III) compounds: α-Fe_3O_4.
   - Aqueous iron species (5 species):
     - Fe (II) compounds: Fe^{+2} and $Fe(OH)_4^{-2}$.
     - Fe (III) compounds: Fe^{+3} and $Fe(OH)_4^-$.
     - Fe (VI) compounds: FeO_4^{-2}.
   - Aqueous iron-bromide species (2 species):
     - Fe (II) compounds: $FeBr_2$(aq).
     - Fe (III) compounds: $FeBr_3$(aq).
2. Species containing chromium (9 chemical species):
   - Solid chromium species (2 species):
     - Metal: Cr.
     - Cr (III) compounds: Cr_2O_3.
   - Aqueous chromium species (6 species):
     - Cr (II) compounds: Cr^{+2}.
     - Cr (III) compounds: Cr^{+3}, $Cr(OH)^{+2}$ and $Cr(OH)_4^-$.
     - Cr (VI) compounds: CrO_4^{-2} and $HCrO_4^-$.
   - Aqueous chromium-bromide species (1 species):
     - Cr (III) compounds: $CrBr^{+2}$.
3. Species containing iron-chromium (1 chemical species):
   - Solid iron-chromium species (1 species):
     - Fe (II)/Cr (III) species: $FeCr_2O_4$.

In the Fe-Cr-H_2O system, aqueous iron-bromide and aqueous chromium-bromide species are not considered. With the three corresponding species removed the number of chemical species in this system is 18.

2.2. Reactions

All the reactions involved in the Fe-Cr-Br^--H_2O system are considered. On the one hand, reactions between iron-chromium species ($FeCr_2O_4$), species containing iron, and species containing chromium are considered. They can be simplified as shown in Eq. (1):

$$FeCr_2O_4 + mH^+ + ne^- + aBr^- \rightleftarrows xX + yY + bH_2O \quad (1)$$

where X is a species containing iron and Y is a species containing chromium.

On the other hand, reactions involving only species containing iron and reactions involving only species containing chromium are also considered, as described by Eqs. (2) and (3), respectively:

$$cX1 + mH^+ + ne^- + aBr^- \rightleftarrows dX2 + bH_2O \quad (2)$$

$$fY1 + mH^+ + ne^- + aBr^- \rightleftarrows gY2 + bH_2O \quad (3)$$

where X1 and X2 are a pair of iron species and Y1 and Y2 are chromium species.

A total of 190 reactions are considered in the Fe-Cr-Br^--H_2O quaternary system. They can be divided into different categories: electrochemical reactions not involving H^+ (21 reactions) and those involving H^+ (126 reactions); chemical reactions involving H^+ (37 reactions) and those not involving H^+ (6 reactions).

Tables 2-5 show the classification of the reactions. Each reaction category is classified into different subcategories: homogeneous reactions (only aqueous species involved) and heterogeneous reactions, involving one, two or three solid species.

Reactions in the Fe-Cr-H_2O system are shaded in grey in Tables 2-5, with the total number of reactions in this particular system being 136.

2.3. Equilibrium conditions

Equilibria for electrochemical and chemical reactions are calculated from data collected at the temperature of 25 ºC of the standard-state Gibbs free energy of formation (ΔG_f^o). These data are compiled in Table 1 for all the chemical species involved [29,49-51], using established methodology [52]. The activity values of aqueous species considered are 10^{-6}, 10^{-4}, 10^{-2} and 10^0.

Bromide ion and water activity values are determined with the thermodynamic model developed by Kusik and Meissner for strong electrolytes in aqueous solutions [53-55], which is described and verified in previous works [44-48]. The bromide ion activities are 15.61, 194.77, 650.06 and 2042.65 and the water activities are 0.715, 0.358, 0.216 and 0.118, corresponding respectively to LiBr/H_2O

Table 2
Electrochemical reactions not involving H^+ for the Fe-Cr-Br^--H_2O system[a].

Type	Equation	Nº
Homogeneous	$Fe^{+3} + e^- \rightleftarrows Fe^{+2}$	1
	$FeBr_3(aq) + e^- \rightleftarrows Fe^{+2} + 3\ Br^-$	2
	$Fe(OH)_4^- + e^- \rightleftarrows Fe(OH)_4^{-2}$	3
	$Fe^{+3} + 2\ Br^- + e^- \rightleftarrows FeBr_2(aq)$	4
	$FeBr_3(aq) + e^- \rightleftarrows FeBr_2(aq) + Br^-$	5
	$Cr^{+3} + e^- \rightleftarrows Cr^{+2}$	6
	$CrBr^{+2} + e^- \rightleftarrows Cr^{+2} + Br^-$	7
Heterogeneous with two solid species	$\mathbf{FeCr_2O_4} + 4\ H_2O + 2\ e^- \rightleftarrows \mathbf{Fe} + 2\ Cr(OH)_4^-$	8
	$\mathbf{FeCr_2O_4} + 2\ e^- \rightleftarrows FeO_4^{-2} + 2\ \mathbf{Cr}$	9
Heterogeneous with one solid species	$Fe^{+3} + 2\ Cr(OH)_4^- + e^- \rightleftarrows \mathbf{FeCr_2O_4} + 4\ H_2O$	10
	$FeO_4^{-2} + 2\ Cr^{+2} + 2\ e^- \rightleftarrows \mathbf{FeCr_2O_4}$	11
	$FeO_4^{-2} + 2\ Cr^{+3} + 4\ e^- \rightleftarrows \mathbf{FeCr_2O_4}$	12
	$FeO_4^{-2} + 2\ CrBr^{+2} + 4\ e^- \rightleftarrows \mathbf{FeCr_2O_4} + 2\ Br^-$	13
	$FeBr_3(aq) + 2\ Cr(OH)_4^- + e^- \rightleftarrows \mathbf{FeCr_2O_4} + 4\ H_2O + 3\ Br^-$	14
	$Fe^{+2} + 2\ e^- \rightleftarrows \mathbf{Fe}$	15
	$Fe^{+3} + 3\ e^- \rightleftarrows \mathbf{Fe}$	16
	$FeBr_2(aq) + 2\ e^- \rightleftarrows \mathbf{Fe} + 2\ Br^-$	17
	$FeBr_3(aq) + 3\ e^- \rightleftarrows \mathbf{Fe} + 3\ Br^-$	18
	$Cr^{+2} + 2\ e^- \rightleftarrows \mathbf{Cr}$	19
	$Cr^{+3} + 3\ e^- \rightleftarrows \mathbf{Cr}$	20
	$CrBr^{+2} + 3\ e^- \rightleftarrows \mathbf{Cr} + Br^-$	21

[a] Solid species are typed in bold letters. Reactions used for the construction of the Pourbaix diagram for the simple Fe-Cr-H_2O system are shaded.

concentrations of 400, 700, 850 and 992 g/L at 25 ºC.

Equilibrium conditions are calculated with a software application developed in previous work [56]. Once the equilibrium conditions are determined, the Pourbaix diagrams (showing the stability zones of the species) and simplified Pourbaix diagrams (showing the zones of immunity, passivation, corrosion, and alkaline corrosion) are represented using AutoCAD software. Diagrams can be challenging to interpret if all the chemical species involved are represented together. For this reason, the decision was made to separate diagrams for iron species and diagrams for chromium species to facilitate analysis of the results. All the stable species that appear in the Pourbaix diagrams are summarised in Tables 6-8.

3. Results and discussion

3.1. Pourbaix diagrams involving iron species for Fe-Cr alloys in LiBr absorption machines

Fig. 1 shows the Pourbaix diagram involving iron species for Fe-Cr alloys in H_2O, which delimits the stability region of solid iron-chromium species $FeCr_2O_4$ together with the solid iron species Fe and Fe_2O_3 and the aqueous iron species Fe^{+2}, $Fe(OH)_4^{-2}$, Fe^{+3}, $Fe(OH)_4^-$ and FeO_4^{-2}. $FeCr_2O_4$ destabilises $Fe(OH)_2$(s) and Fe_3O_4 species, which appeared in the Pourbaix diagram for Fe in H_2O [48].

Metallic Fe forms an immunity zone below the electrochemical equilibrium between water and hydrogen (dashed line labelled “b” in Fig. 1). One consequence is that Fe is a highly reactive metal. Even at an activity value of 10^{-6} for the aqueous iron species, a corrosion region is formed from acid pH to near-neutral pH by Fe^{+2} and Fe^{+3} species, an extensive passivation region is formed from acid to alkaline pH by $FeCr_2O_4$ and Fe_2O_3 species, an alkaline corrosion region is formed at high pH values by $Fe(OH)_4^{-2}$ and $Fe(OH)_4^-$ species, and a wide corrosion region is formed at high potential values by the FeO_4^{-2} species.

The activity value of the aqueous iron species has a crucial effect on the stability regions of the Pourbaix diagram. On the one hand, the size of the corrosion region (stability of aqueous Fe^{+2} and Fe^{+3}) decreases when the activity value is increased from 10^{-6} to 10^0. As a result, the passivation region (stability of solid $FeCr_2O_4$ and Fe_2O_3) and the immunity region (stability of Fe) increase. On the other hand, the alkaline corrosion region at high pH values (stability of aqueous $Fe(OH)_4^{-2}$ and $Fe(OH)_4^-$) extends to higher pHs and lower potentials as activity value increases, with this region disappearing in the Pourbaix diagram for activity values of 10^{-4}, 10^{-2} and 10^0. In addition, increasing the activity value causes the corrosion region to decrease at high potential values (stability of aqueous FeO_4^{-2}).

Figs. 2-5 show the Pourbaix diagrams involving only species containing iron for Fe-Cr alloys in LiBr/H_2O solutions with concentration of 400, 700, 850 and 992 g/L. These diagrams only show the thermodynamic stability zones considering iron and iron-chromium species. In comparison with the Pourbaix diagram in the absence of LiBr (Fig. 1), Fe^{+2} and Fe^{+3} species are not stable in the corrosion region in the presence of LiBr; they are replaced by $FeBr_2$(aq) and $FeBr_3$(aq) species, respectively. The corrosion region shifts to higher pHs and lower potentials when LiBr concentration rises from 400 to 992 g/L, correspondingly increasing the size of this corrosion region. Consequently, the immunity region of Fe and the passivation region of $FeCr_2O_4$ and Fe_2O_3 decrease.

The solid iron-chromium species $FeCr_2O_4$ significantly influences the

Table 3
Electrochemical reactions involving H^+ for the Fe-Cr-Br^--H_2O system[a].

Type	Equation	Nº
Homogeneous	$Fe(OH)_4^- + 4\ H^+ + e^- \rightleftarrows Fe^{+2} + 4\ H_2O$	22
	$FeO_4^{-2} + 8\ H^+ + 4\ e^- \rightleftarrows Fe^{+2} + 4\ H_2O$	23
	$Fe^{+3} + 4\ H_2O + e^- \rightleftarrows Fe(OH)_4^{-2} + 4\ H^+$	24
	$FeO_4^{-2} + 4\ H^+ + 4\ e^- \rightleftarrows Fe(OH)_4^{-2}$	25
	$FeBr_3(aq) + 4\ H_2O + e^- \rightleftarrows Fe(OH)_4^{-2} + 3\ Br^- + 4\ H^+$	26
	$FeO_4^{-2} + 8\ H^+ + 3\ e^- \rightleftarrows Fe^{+3} + 4\ H_2O$	27
	$FeO_4^{-2} + 4\ H^+ + 3\ e^- \rightleftarrows Fe(OH)_4^-$	28
	$Fe(OH)_4^- + 2\ Br^- + 4\ H^+ + e^- \rightleftarrows FeBr_2(aq) + 4\ H_2O$	29
	$FeO_4^{-2} + 2\ Br^- + 8\ H^+ + 4\ e^- \rightleftarrows FeBr_2(aq) + 4\ H_2O$	30
	$FeO_4^{-2} + 3\ Br^- + 8\ H^+ + 3\ e^- \rightleftarrows FeBr_3(aq) + 4\ H_2O$	31
	$CrOH^{+2} + H^+ + e^- \rightleftarrows Cr^{+2} + H_2O$	32
	$Cr(OH)_4^- + 4\ H^+ + e^- \rightleftarrows Cr^{+2} + 4\ H_2O$	33
	$CrO_4^{-2} + 8\ H^+ + 4\ e^- \rightleftarrows Cr^{+2} + 4\ H_2O$	34
	$HCrO_4^- + 7\ H^+ + 4\ e^- \rightleftarrows Cr^{+2} + 4\ H_2O$	35
	$CrO_4^{-2} + 8\ H^+ + 3\ e^- \rightleftarrows Cr^{+3} + 4\ H_2O$	36
	$HCrO_4^- + 7\ H^+ + 3\ e^- \rightleftarrows Cr^{+3} + 4\ H_2O$	37
	$CrO_4^{-2} + 7\ H^+ + 3\ e^- \rightleftarrows CrOH^{+2} + 3\ H_2O$	38
	$HCrO_4^- + 6\ H^+ + 3\ e^- \rightleftarrows CrOH^{+2} + 3\ H_2O$	39
	$CrO_4^{-2} + 4\ H^+ + 3\ e^- \rightleftarrows Cr(OH)_4^-$	40
	$HCrO_4^- + 3\ H^+ + 3\ e^- \rightleftarrows Cr(OH)_4^-$	41
	$CrO_4^{-2} + Br^- + 8\ H^+ + 3\ e^- \rightleftarrows CrBr^{+2} + 4\ H_2O$	42
	$HCrO_4^- + Br^- + 7\ H^+ + 3\ e^- \rightleftarrows CrBr^{+2} + 4\ H_2O$	43
Heterogeneous with three solid species	$\mathbf{FeCr_2O_4} + 8\ H^+ + 8\ e^- \rightleftarrows \mathbf{Fe} + 2\ \mathbf{Cr} + 4\ H_2O$	44
	$\mathbf{FeCr_2O_4} + 2\ H^+ + 2\ e^- \rightleftarrows \mathbf{Fe} + \mathbf{Cr_2O_3} + H_2O$	45
	$\mathbf{FeCr_2O_4} + 6\ H^+ + 6\ e^- \rightleftarrows \mathbf{Fe(OH)_2(s)} + 2\ \mathbf{Cr} + 2\ H_2O$	46
	$3\ \mathbf{FeCr_2O_4} + 16\ H^+ + 16\ e^- \rightleftarrows \mathbf{Fe_3O_4} + 6\ \mathbf{Cr} + 8\ H_2O$	47
	$\mathbf{Fe_3O_4} + 3\ \mathbf{Cr_2O_3} + 2\ H^+ + 2\ e^- \rightleftarrows 3\ \mathbf{FeCr_2O_4} + H_2O$	48
	$2\ \mathbf{FeCr_2O_4} + 10\ H^+ + 10\ e^- \rightleftarrows \mathbf{Fe_2O_3} + 4\ \mathbf{Cr} + 5\ H_2O$	49
	$\mathbf{Fe_2O_3} + 2\ \mathbf{Cr_2O_3} + 2\ H^+ + 2\ e^- \rightleftarrows 2\ \mathbf{FeCr_2O_4} + H_2O$	50

(*continued on next page*)

Table 3 (*continued*)

Type	Equation	Nº
Heterogeneous with two solid species	$\mathbf{FeCr_2O_4} + 8\ H^+ + 4\ e^- \rightleftarrows \mathbf{Fe} + 2\ Cr^{+2} + 4\ H_2O$	51
	$\mathbf{FeCr_2O_4} + 8\ H^+ + 2\ e^- \rightleftarrows \mathbf{Fe} + 2\ Cr^{+3} + 4\ H_2O$	52
	$\mathbf{FeCr_2O_4} + 6\ H^+ + 2\ e^- \rightleftarrows \mathbf{Fe} + 2\ CrOH^{+2} + 2\ H_2O$	53
	$\mathbf{Fe} + 2\ CrO_4^{-2} + 8\ H^+ + 4\ e^- \rightleftarrows \mathbf{FeCr_2O_4} + 4\ H_2O$	54
	$\mathbf{Fe} + 2\ HCrO_4^- + 6\ H^+ + 4\ e^- \rightleftarrows \mathbf{FeCr_2O_4} + 4\ H_2O$	55
	$\mathbf{FeCr_2O_4} + 8\ H^+ + 2\ Br^- + 2\ e^- \rightleftarrows \mathbf{Fe} + 2\ CrBr^{+2} + 4\ H_2O$	56
	$\mathbf{FeCr_2O_4} + 6\ H^+ + 2\ e^- \rightleftarrows \mathbf{Fe(OH)_2(s)} + 2\ Cr^{+2} + 2\ H_2O$	57
	$\mathbf{Fe(OH)_2(s)} + 2\ CrO_4^{-2} + 10\ H^+ + 6\ e^- \rightleftarrows \mathbf{FeCr_2O_4} + 6\ H_2O$	58
	$\mathbf{Fe(OH)_2(s)} + 2\ HCrO_4^- + 8\ H^+ + 6\ e^- \rightleftarrows \mathbf{FeCr_2O_4} + 6\ H_2O$	59
	$3\ \mathbf{FeCr_2O_4} + 16\ H^+ + 4\ e^- \rightleftarrows \mathbf{Fe_3O_4} + 6\ Cr^{+2} + 8\ H_2O$	60
	$\mathbf{Fe_3O_4} + 6\ Cr^{+3} + 8\ H_2O + 2\ e^- \rightleftarrows 3\ \mathbf{FeCr_2O_4} + 16\ H^+$	61
	$\mathbf{Fe_3O_4} + 6\ CrOH^{+2} + 2\ H_2O + 2\ e^- \rightleftarrows 3\ \mathbf{FeCr_2O_4} + 10\ H^+$	62
	$\mathbf{Fe_3O_4} + 6\ Cr(OH)_4^- + 8\ H^+ + 2\ e^- \rightleftarrows 3\ \mathbf{FeCr_2O_4} + 16\ H_2O$	63
	$\mathbf{Fe_3O_4} + 6\ CrO_4^{-2} + 32\ H^+ + 20\ e^- \rightleftarrows 3\ \mathbf{FeCr_2O_4} + 16\ H_2O$	64
	$\mathbf{Fe_3O_4} + 6\ HCrO_4^- + 26\ H^+ + 20\ e^- \rightleftarrows 3\ \mathbf{FeCr_2O_4} + 16\ H_2O$	65
	$\mathbf{Fe_3O_4} + 6\ CrBr^{+2} + 8\ H_2O + 2\ e^- \rightleftarrows 3\ \mathbf{FeCr_2O_4} + 16\ H^+ + 6\ Br^-$	66
	$2\ \mathbf{FeCr_2O_4} + 10\ H^+ + 2\ e^- \rightleftarrows \mathbf{Fe_2O_3} + 4\ Cr^{+2} + 5\ H_2O$	67
	$\mathbf{Fe_2O_3} + 4\ Cr^{+3} + 5\ H_2O + 2\ e^- \rightleftarrows 2\ \mathbf{FeCr_2O_4} + 10\ H^+$	68
	$\mathbf{Fe_2O_3} + 4\ CrOH^{+2} + H_2O + 2\ e^- \rightleftarrows 2\ \mathbf{FeCr_2O_4} + 6\ H^+$	69
	$\mathbf{Fe_2O_3} + 4\ Cr(OH)_4^- + 6\ H^+ + 2\ e^- \rightleftarrows 2\ \mathbf{FeCr_2O_4} + 11\ H_2O$	70
	$\mathbf{Fe_2O_3} + 4\ CrO_4^{-2} + 22\ H^+ + 14\ e^- \rightleftarrows 2\ \mathbf{FeCr_2O_4} + 11\ H_2O$	71
	$\mathbf{Fe_2O_3} + 4\ HCrO_4^- + 18\ H^+ + 14\ e^- \rightleftarrows 2\ \mathbf{FeCr_2O_4} + 11\ H_2O$	72
	$\mathbf{Fe_2O_3} + 4\ CrBr^{+2} + 5\ H_2O + 2\ e^- \rightleftarrows 2\ \mathbf{FeCr_2O_4} + 10\ H^+ + 4\ Br^-$	73
	$\mathbf{FeCr_2O_4} + 8\ H^+ + 6\ e^- \rightleftarrows Fe^{+2} + 2\ \mathbf{Cr} + 4\ H_2O$	74
	$\mathbf{FeCr_2O_4} + 4\ H^+ + 6\ e^- \rightleftarrows Fe(OH)_4^{-2} + 2\ \mathbf{Cr}$	75
	$\mathbf{FeCr_2O_4} + 8\ H^+ + 5\ e^- \rightleftarrows Fe^{+3} + 2\ \mathbf{Cr} + 4\ H_2O$	76
	$Fe^{+3} + \mathbf{Cr_2O_3} + H_2O + e^- \rightleftarrows \mathbf{FeCr_2O_4} + 2\ H^+$	77
	$\mathbf{FeCr_2O_4} + 4\ H^+ + 5\ e^- \rightleftarrows Fe(OH)_4^- + 2\ \mathbf{Cr}$	78
	$Fe(OH)_4^- + \mathbf{Cr_2O_3} + 2\ H^+ + e^- \rightleftarrows \mathbf{FeCr_2O_4} + 3\ H_2O$	79
	$FeO_4^{-2} + \mathbf{Cr_2O_3} + 6\ H^+ + 4\ e^- \rightleftarrows \mathbf{FeCr_2O_4} + 3\ H_2O$	80
	$\mathbf{FeCr_2O_4} + 8\ H^+ + 2\ Br^- + 6\ e^- \rightleftarrows FeBr_2(aq) + 2\ \mathbf{Cr} + 4\ H_2O$	81

(*continued on next page*)

Table 3 (*continued*)

Type	Equation	Nº
Heterogeneous with two solid species	$\mathbf{FeCr_2O_4} + 8\ H^+ + 3\ Br^- + 5\ e^- \rightleftarrows FeBr_3(aq) + 2\ \mathbf{Cr} + 4\ H_2O$	82
	$FeBr_3(aq) + \mathbf{Cr_2O_3} + H_2O + e^- \rightleftarrows \mathbf{FeCr_2O_4} + 2\ H^+ + 3\ Br^-$	83
	$\mathbf{Fe(OH)_2(s)} + 2\ H^+ + 2\ e^- \rightleftarrows \mathbf{Fe} + 2\ H_2O$	84
	$\mathbf{Fe_3O_4} + 8\ H^+ + 8\ e^- \rightleftarrows 3\ \mathbf{Fe} + 4\ H_2O$	85
	$\mathbf{Fe_2O_3} + 6\ H^+ + 6\ e^- \rightleftarrows 2\ \mathbf{Fe} + 3\ H_2O$	86
	$\mathbf{Fe_3O_4} + 2\ H^+ + 2\ H_2O + 2\ e^- \rightleftarrows 3\ \mathbf{Fe(OH)_2(s)}$	87
	$\mathbf{Fe_2O_3} + 2\ H^+ + H_2O + 2e^- \rightleftarrows 2\ \mathbf{Fe(OH)_2(s)}$	88
	$3\ \mathbf{Fe_2O_3} + 2\ H^+ + 2e^- \rightleftarrows 2\ \mathbf{Fe_3O_4} + H_2O$	89
	$\mathbf{Cr_2O_3} + 6\ H^+ + 6\ e^- \rightleftarrows 2\ \mathbf{Cr} + 3\ H_2O$	90
Heterogeneous with one solid species	$\mathbf{FeCr_2O_4} + 8\ H^+ + 2\ e^- \rightleftarrows Fe^{+2} + 2\ Cr^{+2} + 4\ H_2O$	91
	$Fe^{+2} + 2\ CrO_4^{-2} + 8\ H^+ + 6\ e^- \rightleftarrows \mathbf{FeCr_2O_4} + 4\ H_2O$	92
	$Fe^{+2} + 2\ HCrO_4^- + 6\ H^+ + 6\ e^- \rightleftarrows \mathbf{FeCr_2O_4} + 4\ H_2O$	93
	$\mathbf{FeCr_2O_4} + 4\ H^+ + 2\ e^- \rightleftarrows Fe(OH)_4^{-2} + 2\ Cr^{+2}$	94
	$Fe(OH)_4^{-2} + 2\ CrO_4^{-2} + 12\ H^+ + 6\ e^- \rightleftarrows \mathbf{FeCr_2O_4} + 8\ H_2O$	95
	$Fe(OH)_4^{-2} + 2\ HCrO_4^- + 10\ H^+ + 6\ e^- \rightleftarrows \mathbf{FeCr_2O_4} + 8\ H_2O$	96
	$\mathbf{FeCr_2O_4} + 8\ H^+ + e^- \rightleftarrows Fe^{+3} + 2\ Cr^{+2} + 4\ H_2O$	97
	$Fe^{+3} + 2\ Cr^{+3} + 4\ H_2O + e^- \rightleftarrows \mathbf{FeCr_2O_4} + 8\ H^+$	98
	$Fe^{+3} + 2\ CrOH^{+2} + 2\ H_2O + e^- \rightleftarrows \mathbf{FeCr_2O_4} + 6\ H^+$	99
	$Fe^{+3} + 2\ CrO_4^{-2} + 8\ H^+ + 7\ e^- \rightleftarrows \mathbf{FeCr_2O_4} + 4\ H_2O$	100
	$Fe^{+3} + 2\ HCrO_4^- + 6\ H^+ + 7\ e^- \rightleftarrows \mathbf{FeCr_2O_4} + 4\ H_2O$	101
	$Fe^{+3} + 2\ CrBr^{+2} + 4\ H_2O + e^- \rightleftarrows \mathbf{FeCr_2O_4} + 8\ H^+ + 2\ Br^-$	102
	$\mathbf{FeCr_2O_4} + 4\ H^+ + e^- \rightleftarrows Fe(OH)_4^- + 2\ Cr^{+2}$	103
	$Fe(OH)_4^- + 2\ Cr^{+3} + e^- \rightleftarrows \mathbf{FeCr_2O_4} + 4\ H^+$	104
	$Fe(OH)_4^- + 2\ CrOH^{+2} + e^- \rightleftarrows \mathbf{FeCr_2O_4} + 2\ H_2O + 2\ H^+$	105
	$Fe(OH)_4^- + 2\ Cr(OH)_4^- + 4\ H^+ + e^- \rightleftarrows \mathbf{FeCr_2O_4} + 8\ H_2O$	106
	$Fe(OH)_4^- + 2\ CrO_4^{-2} + 12\ H^+ + 7\ e^- \rightleftarrows \mathbf{FeCr_2O_4} + 8\ H_2O$	107
	$Fe(OH)_4^- + 2\ HCrO_4^- + 10\ H^+ + 7\ e^- \rightleftarrows \mathbf{FeCr_2O_4} + 8\ H_2O$	108
	$Fe(OH)_4^- + 2\ CrBr^{+2} + e^- \rightleftarrows \mathbf{FeCr_2O_4} + 4\ H^+ + 2\ Br^-$	109
	$FeO_4^{-2} + 2\ CrOH^{+2} + 2\ H^+ + 4\ e^- \rightleftarrows \mathbf{FeCr_2O_4} + 2\ H_2O$	110
	$FeO_4^{-2} + 2\ Cr(OH)_4^- + 8\ H^+ + 4\ e^- \rightleftarrows \mathbf{FeCr_2O_4} + 8\ H_2O$	111
	$FeO_4^{-2} + 2\ CrO_4^{-2} + 16\ H^+ + 10\ e^- \rightleftarrows \mathbf{FeCr_2O_4} + 8\ H_2O$	112

(*continued on next page*)

Table 3 (*continued*)

Type	Equation	Nº
Heterogeneous with one solid species	$FeO_4^{-2} + 2\,HCrO_4^- + 14\,H^+ + 10\,e^- \rightleftarrows \mathbf{FeCr_2O_4} + 8\,H_2O$	113
	$\mathbf{FeCr_2O_4} + 8\,H^+ + 2\,Br^- + 2\,e^- \rightleftarrows FeBr_2(aq) + 2\,Cr^{+2} + 4\,H_2O$	114
	$FeBr_2(aq) + 2\,CrO_4^{-2} + 8\,H^+ + 6\,e^- \rightleftarrows \mathbf{FeCr_2O_4} + 4\,H_2O + 2\,Br^-$	115
	$FeBr_2(aq) + 2\,HCrO_4^- + 6\,H^+ + 6\,e^- \rightleftarrows \mathbf{FeCr_2O_4} + 4\,H_2O + 2\,Br^-$	116
	$\mathbf{FeCr_2O_4} + 8\,H^+ + 3\,Br^- + e^- \rightleftarrows FeBr_3(aq) + 2\,Cr^{+2} + 4\,H_2O$	117
	$FeBr_3(aq) + 2\,Cr^{+3} + 4\,H_2O + e^- \rightleftarrows \mathbf{FeCr_2O_4} + 8\,H^+ + 3\,Br^-$	118
	$FeBr_3(aq) + 2\,CrOH^{+2} + 2\,H_2O + e^- \rightleftarrows \mathbf{FeCr_2O_4} + 6\,H^+ + 3\,Br^-$	119
	$FeBr_3(aq) + 2\,CrO_4^{-2} + 8\,H^+ + 7\,e^- \rightleftarrows \mathbf{FeCr_2O_4} + 4\,H_2O + 3\,Br^-$	120
	$FeBr_3(aq) + 2\,HCrO_4^- + 6\,H^+ + 7\,e^- \rightleftarrows \mathbf{FeCr_2O_4} + 4\,H_2O + 3\,Br^-$	121
	$FeBr_3(aq) + 2\,CrBr^{+2} + 4\,H_2O + e^- \rightleftarrows \mathbf{FeCr_2O_4} + 8\,H^+ + 5\,Br^-$	122
	$Fe(OH)_4^{-2} + 4\,H^+ + 2\,e^- \rightleftarrows \mathbf{Fe} + 4\,H_2O$	123
	$Fe(OH)_4^- + 4\,H^+ + 3\,e^- \rightleftarrows \mathbf{Fe} + 4\,H_2O$	124
	$FeO_4^{-2} + 8\,H^+ + 6\,e^- \rightleftarrows \mathbf{Fe} + 4\,H_2O$	125
	$Fe^{+3} + 2\,H_2O + e^- \rightleftarrows \mathbf{Fe(OH)_2(s)} + 2\,H^+$	126
	$Fe(OH)_4^- + 2\,H^+ + e^- \rightleftarrows \mathbf{Fe(OH)_2(s)} + 2\,H_2O$	127
	$FeO_4^{-2} + 6\,H^+ + 4\,e^- \rightleftarrows \mathbf{Fe(OH)_2(s)} + 2\,H_2O$	128
	$FeBr_3(aq) + 2\,H_2O + e^- \rightleftarrows \mathbf{Fe(OH)_2(s)} + 3\,Br^- + 2\,H^+$	129
	$\mathbf{Fe_3O_4} + 8\,H^+ + 2\,e^- \rightleftarrows 3\,Fe^{+2} + 4\,H_2O$	130
	$\mathbf{Fe_3O_4} + 8\,H_2O + 2\,e^- \rightleftarrows 3\,Fe(OH)_4^{-2} + 4\,H^+$	131
	$3\,Fe^{+3} + 4\,H_2O + e^- \rightleftarrows \mathbf{Fe_3O_4} + 8\,H^+$	132
	$3\,Fe(OH)_4^- + 4\,H^+ + e^- \rightleftarrows \mathbf{Fe_3O_4} + 8\,H_2O$	133
	$3\,FeO_4^{-2} + 16\,H^+ + 10\,e^- \rightleftarrows \mathbf{Fe_3O_4} + 8\,H_2O$	134
	$\mathbf{Fe_3O_4} + 6\,Br^- + 8\,H^+ + 2e^- \rightleftarrows 3\,FeBr_2(aq) + 4\,H_2O$	135
	$3\,FeBr_3(aq) + 4\,H_2O + e^- \rightleftarrows \mathbf{Fe_3O_4} + 9\,Br^- + 8\,H^+$	136
	$\mathbf{Fe_2O_3} + 6\,H^+ + 2\,e^- \rightleftarrows 2\,Fe^{+2} + 3\,H_2O$	137
	$\mathbf{Fe_2O_3} + 5\,H_2O + 2\,e^- \rightleftarrows 2\,Fe(OH)_4^{-2} + 2\,H^+$	138
	$2\,FeO_4^{-2} + 10\,H^+ + 6\,e^- \rightleftarrows \mathbf{Fe_2O_3} + 5\,H_2O$	139
	$\mathbf{Fe_2O_3} + 4\,Br^- + 6\,H^+ + 2\,e^- \rightleftarrows 2\,FeBr_2(aq) + 3\,H_2O$	140
	$CrOH^{+2} + H^+ + 3\,e^- \rightleftarrows \mathbf{Cr} + H_2O$	141
	$Cr(OH)_4^- + 4\,H^+ + 3\,e^- \rightleftarrows \mathbf{Cr} + 4\,H_2O$	142
	$CrO_4^{-2} + 8\,H^+ + 6\,e^- \rightleftarrows \mathbf{Cr} + 4\,H_2O$	143

Type	Equation	Nº
Heterogeneous with one solid species	$HCrO_4^- + 7\,H^+ + 6\,e^- \rightleftarrows \mathbf{Cr} + 4\,H_2O$	144
	$\mathbf{Cr_2O_3} + 6\,H^+ + 2\,e^- \rightleftarrows 2\,Cr^{+2} + 3\,H_2O$	145
	$2\,CrO_4^{-2} + 10\,H^+ + 6\,e^- \rightleftarrows \mathbf{Cr_2O_3} + 5\,H_2O$	146
	$2\,HCrO_4^- + 8\,H^+ + 6\,e^- \rightleftarrows \mathbf{Cr_2O_3} + 5\,H_2O$	147

[a] Solid species are typed in bold letters. Reactions used for the construction of the Pourbaix diagram for the simple Fe-Cr-H_2O system are shaded.

size of iron species' stability region in the Pourbaix diagrams for Fe-Cr alloys in the presence of LiBr. On the one hand, the formation of $FeCr_2O_4$ destabilises the $Fe(OH)_2$ and Fe_3O_4 species, which appeared in the Pourbaix diagrams for Fe in LiBr/H_2O solutions [48]. On the other hand, the formation of solid $FeCr_2O_4$ significantly affects the size of the stability region of $FeBr_2(aq)$ and $Fe(OH)_4^{-2}$ species.

The chemical reaction between $FeBr_2(aq)$ and $FeCr_2O_4$ is given by Eq. (4), with the equilibrium pH at 25 °C according to Eq. (5):

$$FeCr_2O_4 + 2H^+ + 2Br^- \rightleftarrows FeBr_2(aq) + Cr_2O_3 + H_2O \quad (4)$$

$$pH = \frac{4.056 + 2\log(Br^-) - \log(FeBr_2(aq)) - \log(H_2O)}{2} \quad (5)$$

The equilibrium pH between $FeBr_2(aq)$ and $FeCr_2O_4$ occurs at 6.29,

Table 4
Chemical reactions involving H^+ for the Fe-Cr-Br^--H_2O system[a].

Type	Equation	Nº
Homogeneous	$Fe^{+2} + 4\ H_2O \rightleftarrows Fe(OH)_4^{-2} + 4\ H^+$	148
	$FeBr_2(aq) + 4\ H_2O \rightleftarrows Fe(OH)_4^{-2} + 2\ Br^- + 4\ H^+$	149
	$Fe^{+3} + 4\ H_2O \rightleftarrows Fe(OH)_4^- + 4\ H^+$	150
	$FeBr_3(aq) + 4\ H_2O \rightleftarrows Fe(OH)_4^- + 3\ Br^- + 4\ H^+$	151
	$Cr^{+3} + H_2O \rightleftarrows CrOH^{+2} + H^+$	152
	$Cr^{+3} + 4\ H_2O \rightleftarrows Cr(OH)_4^- + 4\ H^+$	153
	$CrOH^{+2} + 3\ H_2O \rightleftarrows Cr(OH)_4^- + 3\ H^+$	154
	$CrOH^{+2} + Br^- + H^+ \rightleftarrows CrBr^{+2} + H_2O$	155
	$Cr(OH)_4^- + Br^- + 4\ H^+ \rightleftarrows CrBr^{+2} + 4\ H_2O$	156
	$CrO_4^{-2} + H^+ \rightleftarrows HCrO_4^-$	157
Heterogeneous with two solid species	$\mathbf{FeCr_2O_4} + 6\ H^+ \rightleftarrows \mathbf{Fe(OH)_2(s)} + 2\ Cr^{+3} + 2\ H_2O$	158
	$\mathbf{FeCr_2O_4} + 4\ H^+ \rightleftarrows \mathbf{Fe(OH)_2(s)} + 2\ CrOH^{+2}$	159
	$\mathbf{FeCr_2O_4} + 6\ H_2O \rightleftarrows \mathbf{Fe(OH)_2(s)} + 2\ Cr(OH)_4^- + 2\ H^+$	160
	$\mathbf{FeCr_2O_4} + 6\ H^+ + 2\ Br^- \rightleftarrows \mathbf{Fe(OH)_2(s)} + 2\ CrBr^{+2} + 2\ H_2O$	161
	$\mathbf{FeCr_2O_4} + 2\ H^+ \rightleftarrows Fe^{+2} + \mathbf{Cr_2O_3} + H_2O$	162
	$\mathbf{FeCr_2O_4} + 3\ H_2O \rightleftarrows Fe(OH)_4^{-2} + \mathbf{Cr_2O_3} + 2\ H^+$	163
	$\mathbf{FeCr_2O_4} + 2\ H^+ + 2\ Br^- \rightleftarrows FeBr_2(aq) + \mathbf{Cr_2O_3} + H_2O$	164
Heterogeneous with one solid species	$\mathbf{FeCr_2O_4} + 8\ H^+ \rightleftarrows Fe^{+2} + 2\ Cr^{+3} + 4\ H_2O$	165
	$\mathbf{FeCr_2O_4} + 6\ H^+ \rightleftarrows Fe^{+2} + 2\ CrOH^{+2} + 2\ H_2O$	166
	$\mathbf{FeCr_2O_4} + 8\ H^+ + 2\ Br^- \rightleftarrows Fe^{+2} + 2\ CrBr^{+2} + 4\ H_2O$	167
	$\mathbf{FeCr_2O_4} + 4\ H^+ \rightleftarrows Fe(OH)_4^{-2} + 2\ Cr^{+3}$	168
	$\mathbf{FeCr_2O_4} + 2\ H_2O + 2\ H^+ \rightleftarrows Fe(OH)_4^{-2} + 2\ CrOH^{+2}$	169
	$\mathbf{FeCr_2O_4} + 8\ H_2O \rightleftarrows Fe(OH)_4^{-2} + 2\ Cr(OH)_4^- + 4\ H^+$	170
	$\mathbf{FeCr_2O_4} + 4\ H^+ + 2\ Br^- \rightleftarrows Fe(OH)_4^{-2} + 2\ CrBr^{+2}$	171
	$\mathbf{FeCr_2O_4} + 8\ H^+ + 2\ Br^- \rightleftarrows FeBr_2(aq) + 2\ Cr^{+3} + 4\ H_2O$	172
	$\mathbf{FeCr_2O_4} + 6\ H^+ + 2\ Br^- \rightleftarrows FeBr_2(aq) + 2\ CrOH^{+2} + 2\ H_2O$	173
	$\mathbf{FeCr_2O_4} + 8\ H^+ + 4\ Br^- \rightleftarrows FeBr_2(aq) + 2\ CrBr^{+2} + 4\ H_2O$	174
	$Fe^{+2} + 2\ H_2O \rightleftarrows \mathbf{Fe(OH)_2(s)} + 2\ H^+$	175
	$\mathbf{Fe(OH)_2(s)} + 2\ H_2O \rightleftarrows Fe(OH)_4^{-2} + 2\ H^+$	176
	$FeBr_2(aq) + 2\ H_2O \rightleftarrows \mathbf{Fe(OH)_2(s)} + 2\ Br^- + 2\ H^+$	177

Type	Equation	Nº
Heterogeneous with one solid species	$2\ Fe^{+3} + 3\ H_2O \rightleftarrows \mathbf{Fe_2O_3} + 6\ H^+$	178
	$\mathbf{Fe_2O_3} + 5\ H_2O \rightleftarrows 2\ Fe(OH)_4^- + 2\ H^+$	179
	$2\ FeBr_3(aq) + 3\ H_2O \rightleftarrows \mathbf{Fe_2O_3} + 6\ Br^- + 6\ H^+$	180
	$\mathbf{Cr_2O_3} + 6\ H^+ \rightleftarrows 2\ Cr^{+3} + 3\ H_2O$	181
	$\mathbf{Cr_2O_3} + 4\ H^+ \rightleftarrows 2\ CrOH^{+2} + H_2O$	182
	$\mathbf{Cr_2O_3} + 5\ H_2O \rightleftarrows 2\ Cr(OH)_4^- + 2\ H^+$	183
	$\mathbf{Cr_2O_3} + 2\ Br^- + 6\ H^+ \rightleftarrows 2\ CrBr^{+2} + 3\ H_2O$	184

[a] Solid species are typed in bold letters. Reactions used for the construction of the Pourbaix diagram for the simple Fe-Cr-H_2O system are shaded.

Table 5
Chemical reactions not involving H^+ for the Fe-Cr-Br^--H_2O system[a].

Type	Equation	Nº
Homogeneous	$Fe^{+2} + 2\ Br^- \rightleftarrows FeBr_2(aq)$	185
	$Fe^{+3} + 3\ Br^- \rightleftarrows FeBr_3(aq)$	186
	$Cr^{+3} + Br^- \rightleftarrows CrBr^{+2}$	187
Heterogeneous with three solid species	$\mathbf{FeCr_2O_4} + H_2O \rightleftarrows \mathbf{Fe(OH)_2(s)} + \mathbf{Cr_2O_3}$	188
Heterogeneous with one solid species	$\mathbf{FeCr_2O_4} + 4\ H_2O \rightleftarrows Fe^{+2} + 2\ Cr(OH)_4^-$	189
	$\mathbf{FeCr_2O_4} + 4\ H_2O + 2\ Br^- \rightleftarrows FeBr_2(aq) + 2\ Cr(OH)_4^-$	190

[a] Solid species are typed in bold letters. Reactions used for the construction of the Pourbaix diagram for the simple Fe-Cr-H_2O system are shaded.

Table 6
Thermodynamic stability of species for the Fe-Cr-Br^--H_2O system in aqueous solutions with high concentration of LiBr, at an activity value of 10^{-6} for the aqueous species[a].

Species	$(Br^-) = 0$ $(H_2O) = 1$ [LiBr] = 0 g/L	$(Br^-) = 15.61$ $(H_2O) = 0.715$ [LiBr] = 400 g/L	$(Br^-) = 194.77$ $(H_2O) = 0.358$ [LiBr] = 700 g/L	$(Br^-) = 650.06$ $(H_2O) = 0.216$ [LiBr] = 850 g/L	$(Br^-) = 2042.65$ $(H_2O) = 0.118$ [LiBr] = 992 g/L
Fe	I	I	I	I	I
$Fe(OH)_2(s)$					
α-Fe_3O_4					
α-Fe_2O_3	I	I	I	I	I
Fe^{+2}	I				
$Fe(OH)_4^{-2}$	I	I			
Fe^{+3}	I				
$Fe(OH)_4^-$	I	I			
FeO_4^{-2}	I	I	I	I	I
Cr	C	C	C	C	C
Cr_2O_3	C	C	C	C	C
Cr^{+2}	C	C	C	C	C
Cr^{+3}	C	C	C	C	
$CrOH^{+2}$	C	C	C	C	C
$Cr(OH)_4^-$	C	C	C	C	C
CrO_4^{-2}	C	C	C	C	C
$HCrO_4^-$	C	C	C	C	C
$FeCr_2O_4$	I C	I C	I C	I C	I C
$FeBr_2(aq)$		I	I	I	I
$FeBr_3(aq)$		I	I	I	I
$CrBr^{+2}$					C

[a] I = it appears in the Pourbaix diagram of iron species; C = it appears in the Pourbaix diagram of chromium species.

7.54, 8.17 and 8.80, corresponding to LiBr concentrations in H_2O of 400, 700, 850 and 992 g/L, respectively, at an activity of 10^{-6} for the aqueous species, as shown by the lines labelled "164″ in Figs. 2-5. It should be noted that the higher the LiBr concentration, the higher the Br^- activity and the lower the H_2O activity. Therefore, the corrosion region of $FeBr_2$(aq) shifts from acid pH to alkaline pH with increasing LiBr concentration, while the passivation region of $FeCr_2O_4$ shrinks, as shown in Figs. 2-5. In contrast, the equilibrium pH between Fe^{+2} and $FeCr_2O_4$ occurs at 6.17 in the absence of LiBr, at an activity value of 10^{-6} for the aqueous species and H_2O activity of 1, as shown by the line labelled "162″ in Fig. 1.

The chemical reaction between $FeCr_2O_4$ and $Fe(OH)_4^{-2}$ is given by Eq. (6), with the equilibrium at 25 ºC according to Eq. (7):

$$FeCr_2O_4 + 8H_2O \rightleftarrows Fe(OH)_4^{-2} + 2Cr(OH)_4^- + 4H^+ \quad (6)$$

$$pH = \frac{\log\left(Fe(OH)_4^{-2}\right) + 2\log\left(Cr(OH)_4^-\right) - 8\log\left(H_2O\right) + 79.889}{4} \quad (7)$$

At an activity value of 10^{-6} for the aqueous species, the equilibrium pH between $FeCr_2O_4$ and $Fe(OH)_4^{-2}$ occurs at pH values of 15.76, 16.36, 16.80 and 17.33, which correspond respectively to LiBr concentrations in H_2O of 400, 700, 850 and 992 g/L. Therefore, the alkaline corrosion of $Fe(OH)_4^{-2}$ shifts to higher pHs by increasing LiBr concentration. This region is only shown in the sole case of the Pourbaix diagram in LiBr/H_2O solution of 400 g/L (Fig. 2), with the equilibrium pH represented by the line labelled "170″. In the absence of LiBr, equilibrium pH between $FeCr_2O_4$ and $Fe(OH)_4^{-2}$ occurs at 15.47 at an activity value of 10^{-6} for the aqueous species and H_2O activity of 1, as shown by the line labelled "170″ in Fig. 1.

Regarding the $Fe(OH)_4^-$ species, its alkaline corrosion region moves to higher pHs when LiBr concentration is increased (and H_2O activity is decreased), at an activity value of 10^{-6} for the aqueous species. This region only appears in the Pourbaix diagram in LiBr/H_2O solution of 400 g/L (Fig. 2).

Finally, the corrosion region at high potential values of FeO_4^{-2} moves to higher pHs and potentials by increasing LiBr concentration due to the decrease of H_2O activity, as shown in Figs. 2-5. Therefore, the size of this corrosion region decreases when LiBr concentration is increased.

In relation to the effect of the activity value of the aqueous iron species on the Pourbaix diagrams in the presence of LiBr, it can be

Table 7
Thermodynamic stability of species for the Fe-Cr-Br^--H_2O system in aqueous solutions with high concentration of LiBr, at an activity value of 10^{-4} for the aqueous species[a].

Species	(Br^-) = 0 (H_2O) = 1 [LiBr] = 0 g/L	(Br^-) = 15.61 (H_2O) = 0.715 [LiBr] = 400 g/L	(Br^-) = 194.77 (H_2O) = 0.358 [LiBr] = 700 g/L	(Br^-) = 650.06 (H_2O) = 0.216 [LiBr] = 850 g/L	(Br^-) = 2042.65 (H_2O) = 0.118 [LiBr] = 992 g/L
Fe	I	I	I	I	I
$Fe(OH)_2$(s)					
α-Fe_3O_4					
α-Fe_2O_3	I	I	I	I	I
Fe^{+2}	I				
$Fe(OH)_4^{-2}$					
Fe^{+3}	I				
$Fe(OH)_4^-$					
FeO_4^{-2}	I	I	I	I	I
Cr	C	C	C	C	C
Cr_2O_3	C	C	C	C	C
Cr^{+2}	C	C	C	C	C
Cr^{+3}	C	C	C	C	
$CrOH^{+2}$	C	C	C	C	
$Cr(OH)_4^-$	C	C			
CrO_4^{-2}	C	C	C	C	C
$HCrO_4^-$	C	C	C	C	C
$FeCr_2O_4$	I C	I C	I C	I C	I C
$FeBr_2$(aq)		I	I	I	I
$FeBr_3$(aq)		I	I	I	I
$CrBr^{+2}$					C

[a] I = it appears in the Pourbaix diagram of iron species; C = it appears in the Pourbaix diagram of chromium species.

Table 8
Thermodynamic stability of species for the Fe-Cr-Br^--H_2O system in aqueous solutions with high concentration of LiBr, at activity values of 10^{-2} and 10^0 for the aqueous species[a].

Species	(Br^-) = 0 (H_2O) = 1 [LiBr] = 0 g/L	(Br^-) = 15.61 (H_2O) = 0.715 [LiBr] = 400 g/L	(Br^-) = 194.77 (H_2O) = 0.358 [LiBr] = 700 g/L	(Br^-) = 650.06 (H_2O) = 0.216 [LiBr] = 850 g/L	(Br^-) = 2042.65 (H_2O) = 0.118 [LiBr] = 992 g/L
Fe	I	I	I	I	I
$Fe(OH)_2$(s)					
α-Fe_3O_4					
α-Fe_2O_3	I	I	I	I	I
Fe^{+2}	I				
$Fe(OH)_4^{-2}$					
Fe^{+3}	I				
$Fe(OH)_4^-$					
FeO_4^{-2}	I	I	I	I	I
Cr	C	C	C	C	C
Cr_2O_3	C	C	C	C	C
Cr^{+2}	C	C	C	C	C
Cr^{+3}	C	C	C	C	
$CrOH^{+2}$					
$Cr(OH)_4^-$					
CrO_4^{-2}	C	C	C	C	C
$HCrO_4^-$	C	C	C	C	C
$FeCr_2O_4$	I C	I C	I C	I C	I C
$FeBr_2$(aq)		I	I	I	I
$FeBr_3$(aq)		I	I	I	I
$CrBr^{+2}$					C

[a] I = it appears in the Pourbaix diagram of iron species; C = it appears in the Pourbaix diagram of chromium species.

deduced that the size of the corrosion region due to $FeBr_2$(aq) and $FeBr_3$(aq) decreases when activity value is increased from 10^{-6} to 10^0. One consequence of this is the increase in the size of the immunity region of Fe and in the passivation region of $Fe_2Cr_2O_4$ and Fe_2O_3. The activity value's effect on the alkaline corrosion region at high pH values due to $Fe(OH)_4^{-2}$ and $Fe(OH)_4^-$ and on the corrosion region at high potential values of FeO_4^{-2} is similar to that described earlier in the discussion of the Pourbaix diagram in the absence of LiBr.

3.2. Pourbaix diagrams involving chromium species for Fe-Cr alloys in LiBr absorption machines

Fig. 6 shows the Pourbaix diagram involving chromium species for Fe-Cr alloys in H_2O, which delimits the stability region of solid iron-chromium species $FeCr_2O_4$ together with the solid chromium species Cr and Cr_2O_3 and the aqueous chromium species Cr^{+2}, Cr^{+3}, $CrOH^{+2}$, $Cr(OH)_4^-$, CrO_4^{-2} and $HCrO_4^-$. Species containing chromium are the same as those exhibited in the Pourbaix diagram of Cr in H_2O [46].

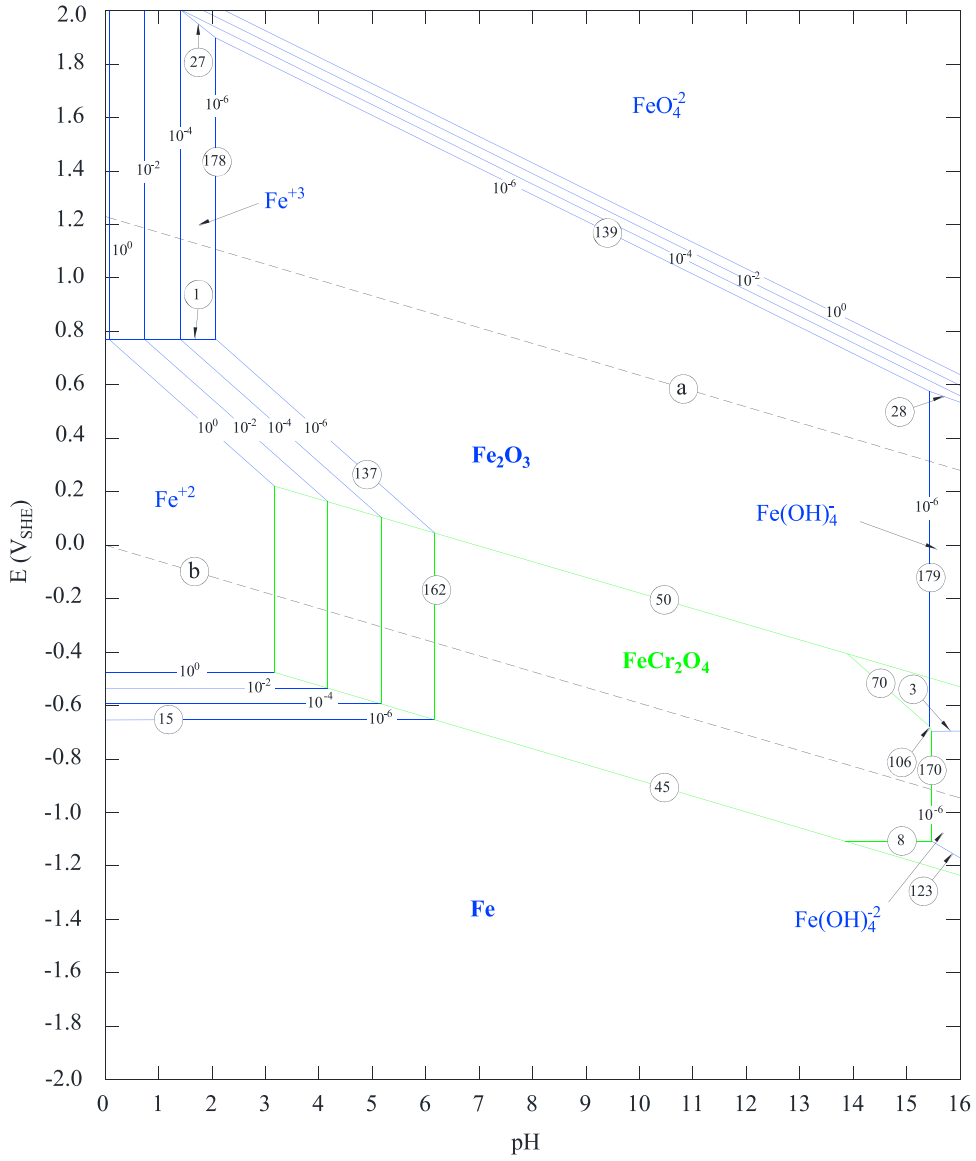

Fig. 1. Pourbaix diagram involving iron species for Fe-Cr alloys in H_2O.

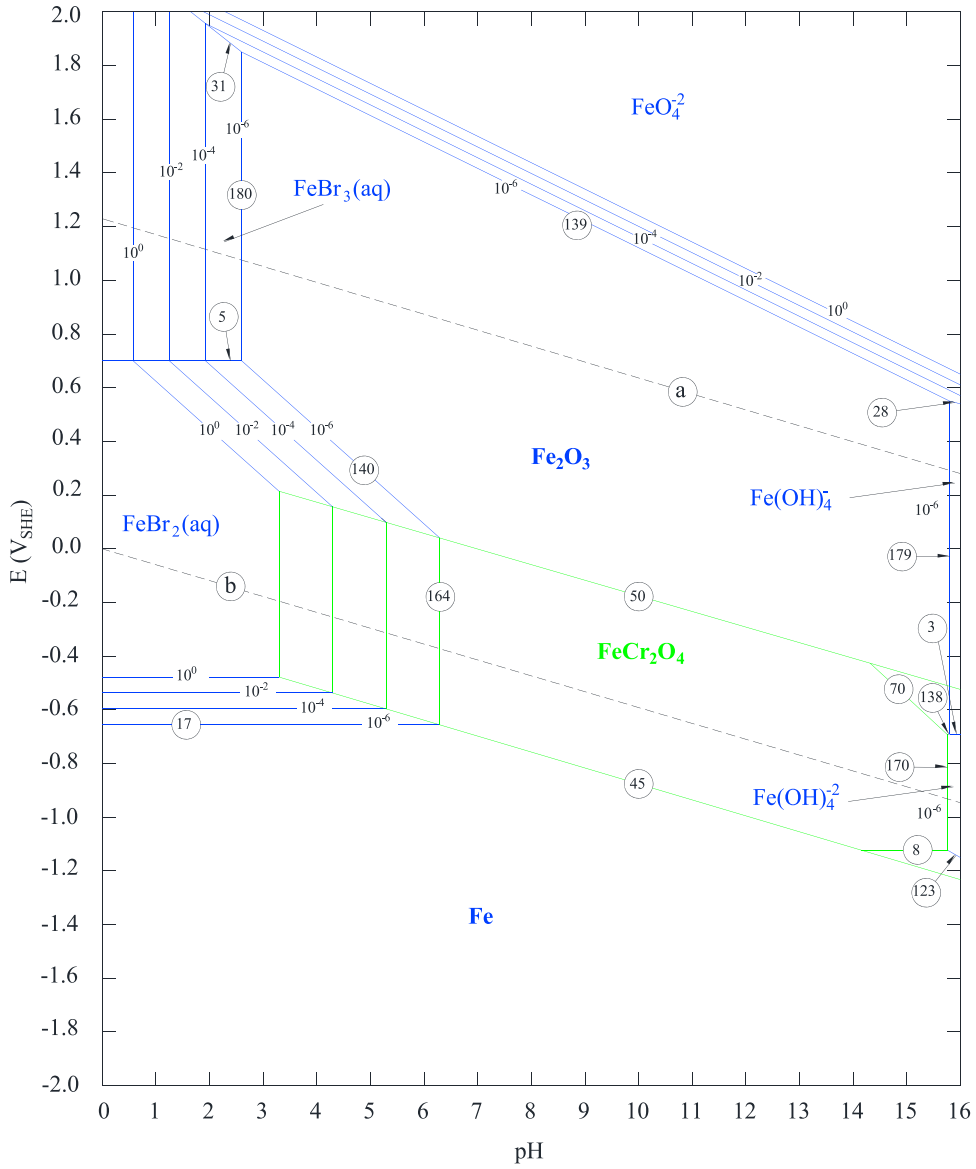

Fig. 2. Pourbaix diagram involving iron species for Fe-Cr alloys in LiBr/H_2O solution of 400 g/L.

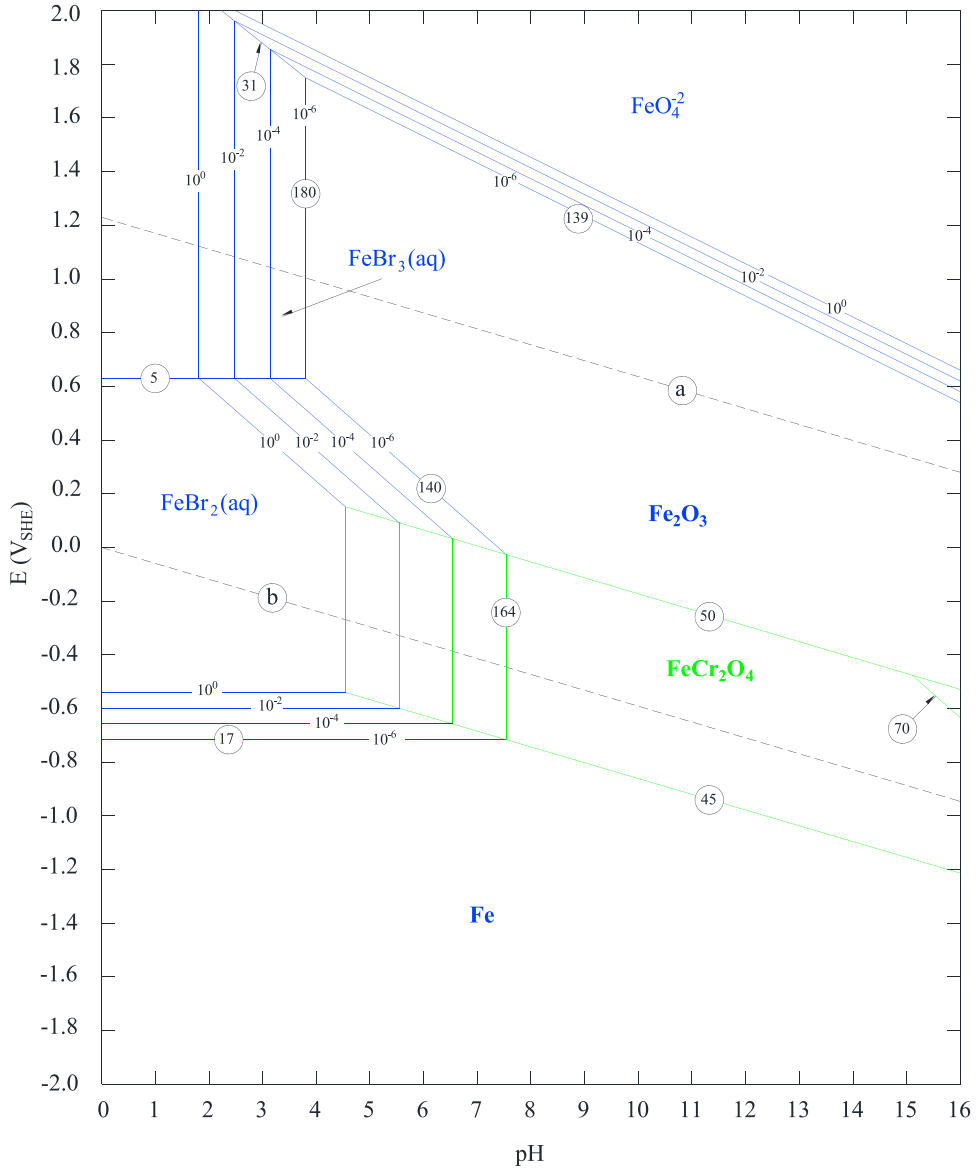

Fig. 3. Pourbaix diagram involving iron species for Fe-Cr alloys in LiBr/H_2O solution of 700 g/L.

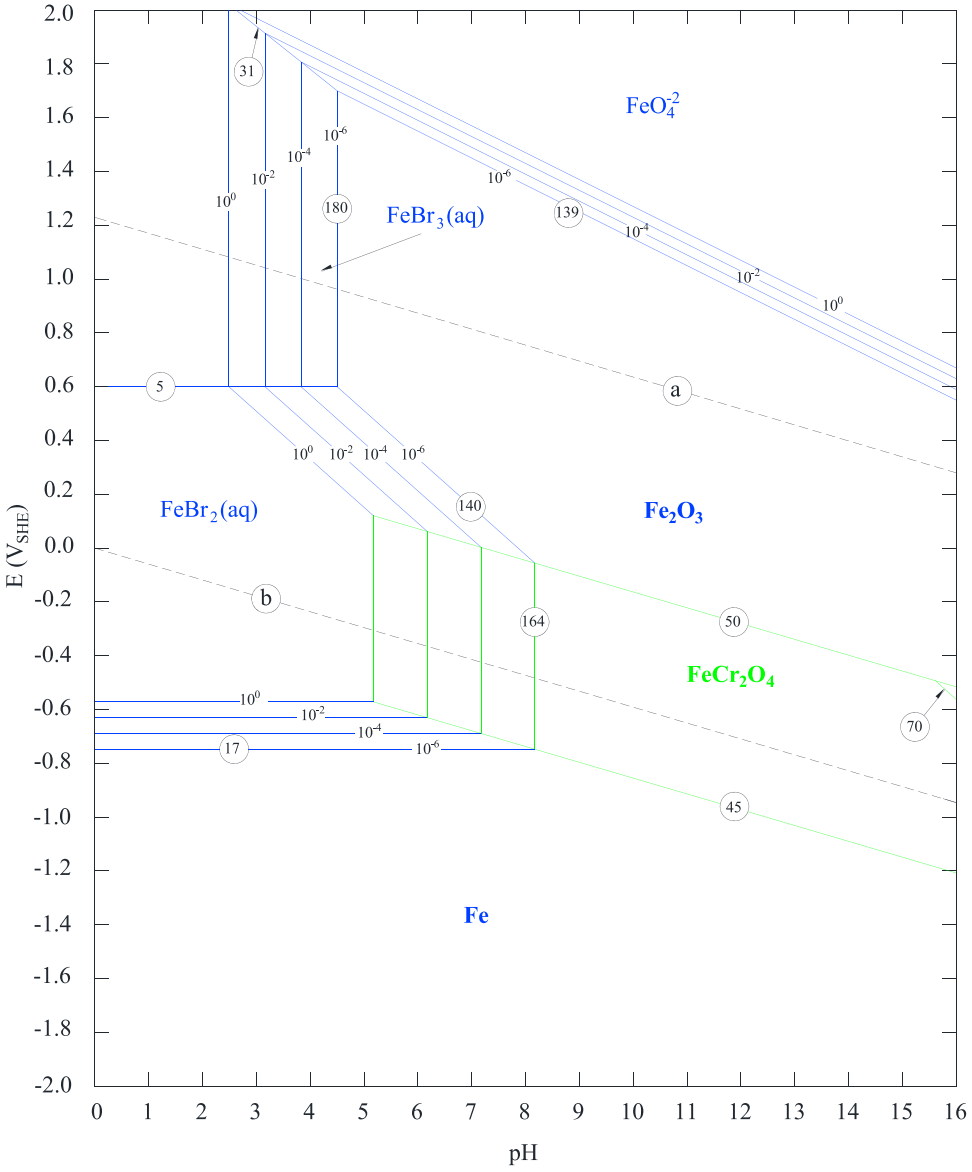

Fig. 4. Pourbaix diagram involving iron species for Fe-Cr alloys in $LiBr/H_2O$ solution of 850 g/L.

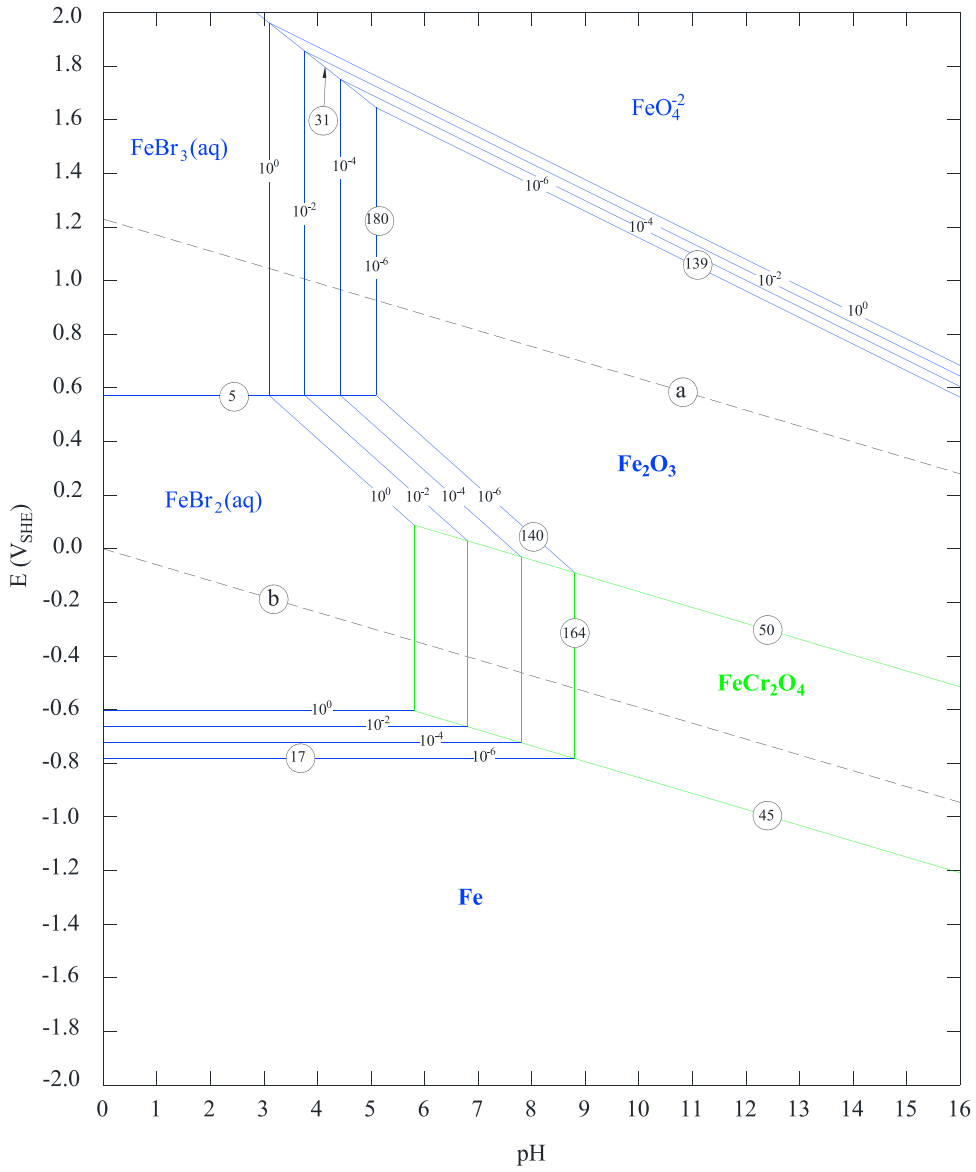

Fig. 5. Pourbaix diagram involving iron species for Fe-Cr alloys in LiBr/H_2O solution of 992 g/L.

The immunity zone (stability of Cr) is located below the electrochemical equilibrium between H_2O and H_2, marked in Fig. 6 with the dashed line "b". Hence, Cr is a highly reactive metal. Cr can oxidize to form the aqueous chromium species Cr^{+2} and $Cr(OH)_4^-$ and the solid chromium species Cr_2O_3. Even at an activity value of 10^{-6} for the aqueous chromium species, a corrosion zone is formed from acid pH to neutral pH by the Cr^{+2} species, a wide passivation zone is formed by the Cr_2O_3 species, and an alkaline corrosion zone is formed at high pH values by the $Cr(OH)_4^-$ species. Solid $FeCr_2O_4$ forms a new passivation zone inside the stability zone of Cr_2O_3, which reaches higher pH values and partially occupies the alkaline corrosion zone of $Cr(OH)_4^-$. The aqueous species Cr^{+2} is unstable at higher potential values and it can oxidize to the aqueous Cr(III) species (Cr^{+3} and $CrOH^{+2}$), which form a corrosion zone at acid pH. Finally, the Cr(III) species (Cr^{+3}, $CrOH^{+2}$, Cr_2O_3, and $Cr(OH)_4^-$) can oxidize to the aqueous Cr(VI) species ($HCrO_4^-$ and CrO_4^{-2}), which form a wide corrosion zone at high potential values.

It should be noted that the stability zone of the species in the Pourbaix diagram depends on the activity value of the aqueous chromium species. On the one hand, the dimensions of the corrosion zone at acid and neutral pH (stability of Cr^{+2}, Cr^{+3}, and $CrOH^{+2}$) and the corrosion zone at high potential values (stability of $HCrO_4^-$ and CrO_4^{-2}) decrease when the activity value is increased from 10^{-6} to 10^{0}. The $CrOH^{+2}$ species is unstable at 10^{-2} and 10^{0} activity values. The alkaline corrosion zone at high pH values (stability of $Cr(OH)_4^-$) extends to higher potential and pH values by increasing activity value, with this zone disappearing in the Pourbaix diagram for activity values of 10^{-2} and 10^{0}. On the other hand, the immunity zone (stability of Cr) and the passivation zone (stability of Cr_2O_3 and $FeCr_2O_4$) increase when the activity value is increased.

Figs. 7-10 show Pourbaix diagrams involving only species containing chromium for Fe-Cr alloys in LiBr/H_2O solutions with concentrations of 400, 700, 850 and 992 g/L. The figures only show the thermodynamic stability zones when chromium and iron-chromium species are considered. In comparison with the Pourbaix diagram in the absence of LiBr (Fig. 6), Cr^{+2}, Cr^{+3} and $CrOH^{+2}$ remain stable in the corrosion zone at acid and neutral pH in the presence of LiBr. An exception comes in the Pourbaix diagram in LiBr/H_2O solution of 992 g/L, where Cr^{+2}, $CrBr^{+2}$ and $CrOH^{+2}$ are the stable species since Cr^{+3} is not stable. The corrosion zone extends to higher pHs when LiBr concentration rises from 400 to 992 g/L, increasing the dimensions of the corrosion zone. Consequently, the immunity zone of Cr and the passivation zone of Cr_2O_3 decrease slightly.

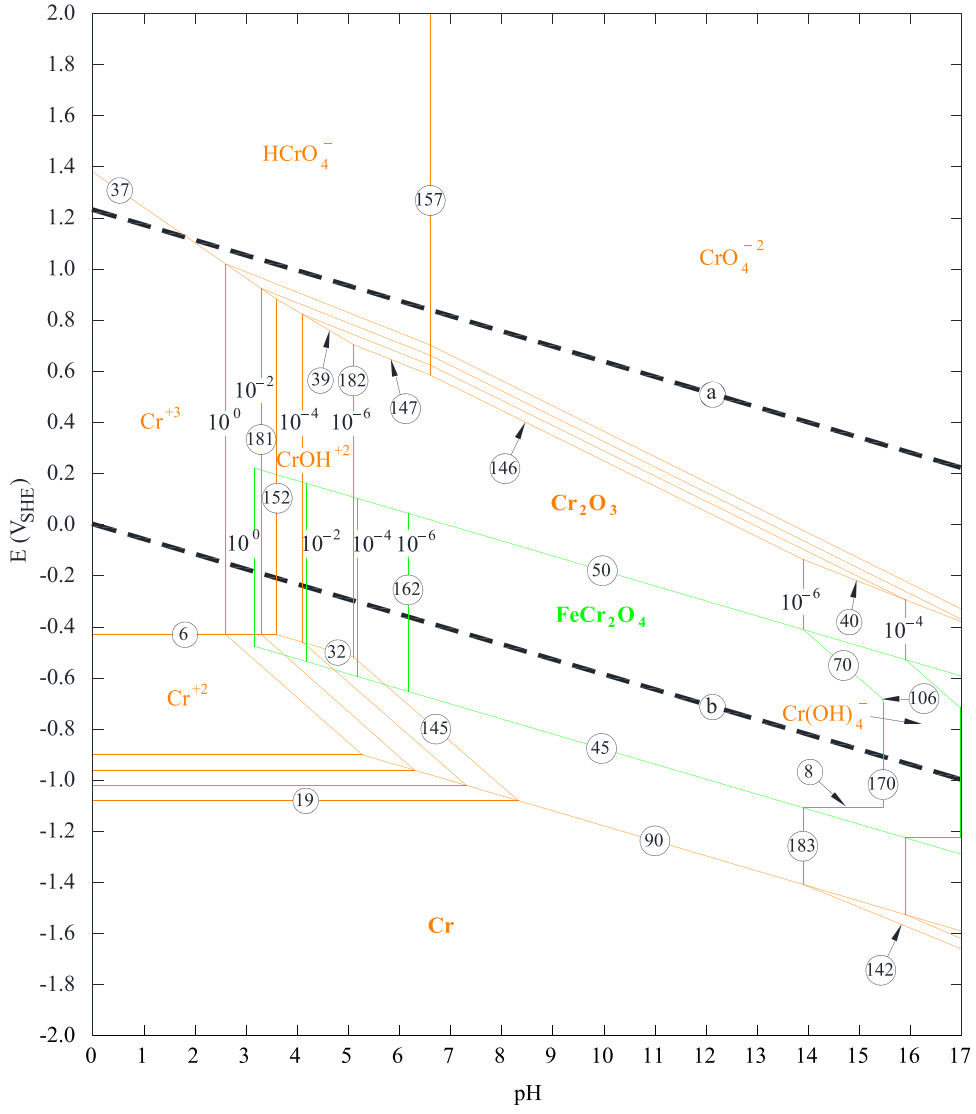

Fig. 6. Pourbaix diagram involving chromium species for Fe-Cr alloys in H_2O.

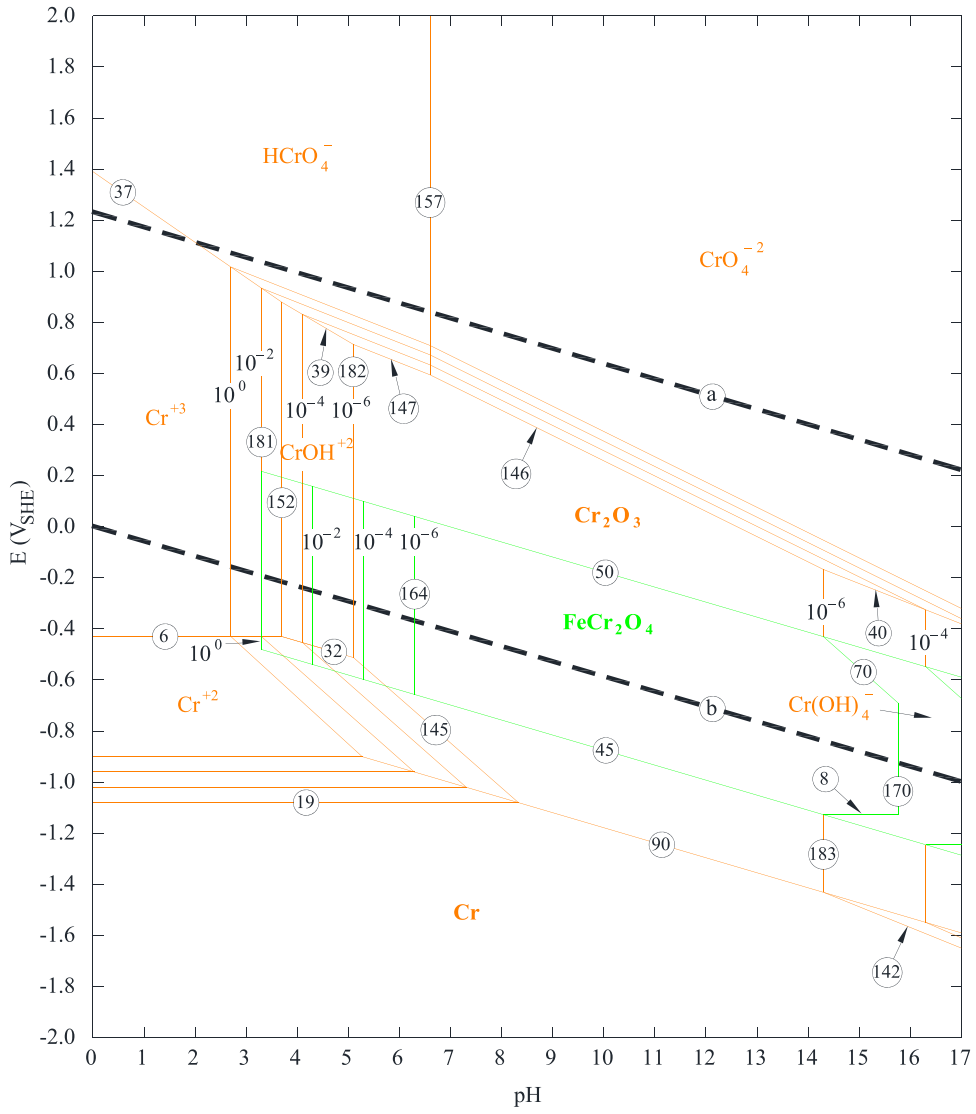

Fig. 7. Pourbaix diagram involving chromium species for Fe-Cr alloys in LiBr/H_2O solution of 400 g/L.

The formation of $FeCr_2O_4$ in the Pourbaix diagrams for Fe-Cr alloys in the presence of LiBr substantially affects the dimensions of the alkaline corrosion zone of $Cr(OH)_4^-$. Equilibrium between $FeCr_2O_4$ and $Cr(OH)_4^-$ is given by the chemical reaction indicated previously in Eq. (6) and the electrochemical reactions shown in Eqs. (8) and (10), with the equilibrium conditions at 25 °C for each reaction shown in Eqs. (7), (9) and (11), respectively:

$$FeCr_2O_4 + 4H_2O + 2e^- \rightleftarrows Fe + 2Cr(OH)_4^- \quad (8)$$

$$E(V_{SHE}) = -1.466 + 0.0296 \log\left[\frac{(H_2O)^4}{(Cr(OH)_4^-)^2}\right] \quad (9)$$

$$Fe_2O_3 + 4Cr(OH)_4^- + 6H^+ + 2e^- \rightleftarrows 2FeCr_2O_4 + 11H_2O \quad (10)$$

$$E(V_{SHE}) = 2.763 + 0.0296 \log\left[\frac{(Cr(OH)_4^-)^4}{(H_2O)^{11}}\right] - 0.177\,pH \quad (11)$$

These equilibria are represented by the lines labelled "170″, "8″, and "70″ in Figs. 7-10. By increasing LiBr concentration (which is equivalent to decreasing H_2O activity) the passivation zone of $FeCr_2O_4$ extends to lower potentials and higher pHs, considering the activity of 10^{-6} for the aqueous species. Consequently, the dimensions of the alkaline corrosion zone of $Cr(OH)_4^-$ decrease significantly.

Finally, the corrosion zone at high potentials of $HCrO_4^-$ and CrO_4^{-2} shifts to higher potentials and pHs by increasing LiBr concentration due to decreased H_2O activity, as shown in Figs. 7-10. Therefore, the dimensions of this zone decrease slightly when LiBr concentration is increased.

In relation to the effect of the activity value of the aqueous chromium species on the Pourbaix diagrams in the presence of LiBr, it can be deduced that the size of the corrosion zone of Cr^{+2}, $CrOH^{+2}$, Cr^{+3} or $CrBr^{+2}$ decreases when activity value is increased from 10^{-6} to 10^{0}. Consequently, the immunity zone of Cr and the passivation zone of Cr_2O_3 increase. The $CrOH^{+2}$ species remain unstable for activity values of 10^{-2} and 10^{0} in the presence of LiBr, whereas it is also not stable for an activity value of 10^{-4} in the case of the LiBr/H_2O solution of 992 g/L. The effect of activity value on the alkaline corrosion zone of $Cr(OH)_4^-$ and on the corrosion zone at high potentials of $HCrO_4^-$ and CrO_4^{-2} is similar to that described above in the discussion of the Pourbaix diagram in the absence of LiBr. The alkaline corrosion zone of $Cr(OH)_4^-$ appears with 10^{-6} and 10^{-4} activity values in the Pourbaix diagram for Fe-Cr alloys in LiBr/H_2O solution of 400 g/L (Fig. 7), whereas it only appears with an activity value of 10^{-6} in the Pourbaix diagrams for Fe-Cr alloys in LiBr/H_2O solutions of 700, 850 and 992 g/L (Figs. 8-10).

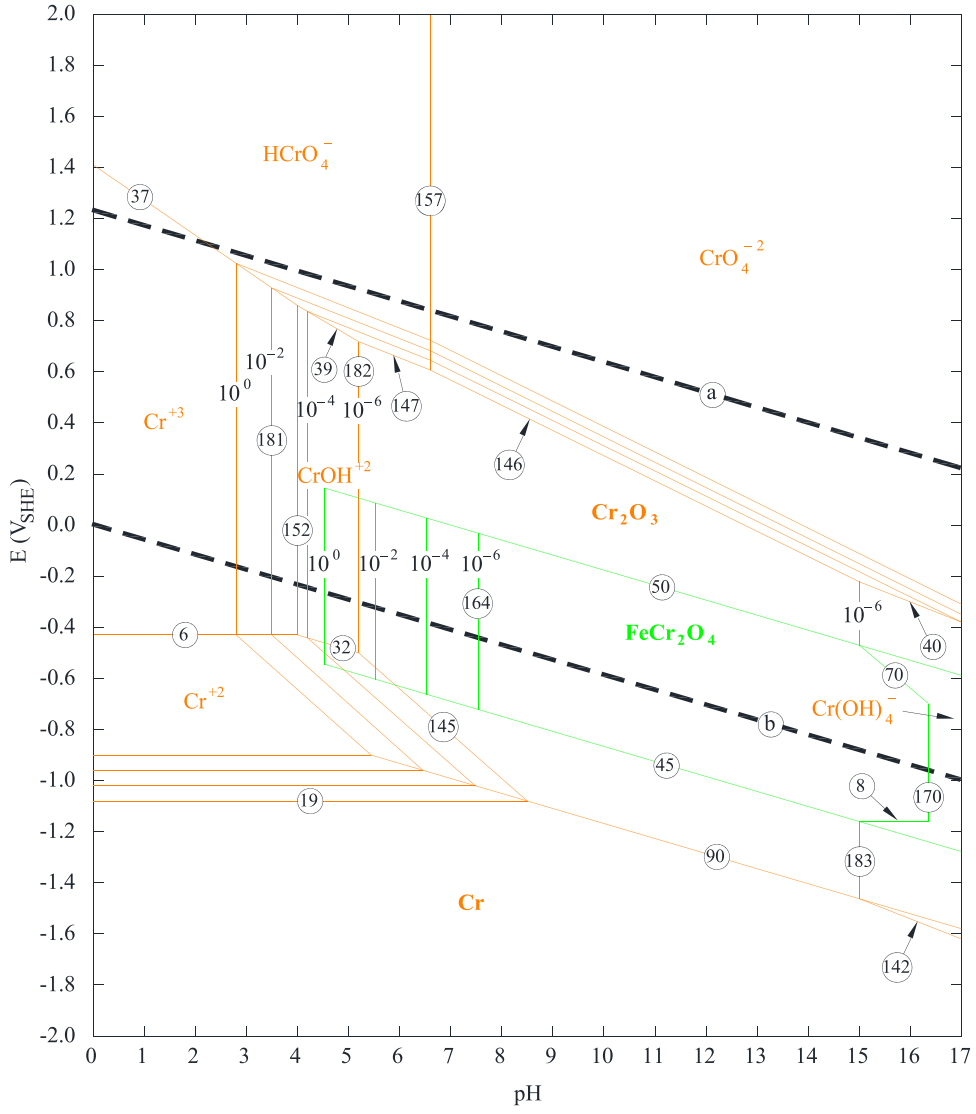

Fig. 8. Pourbaix diagram involving chromium species for Fe-Cr alloys in LiBr/H_2O solution of 700 g/L.

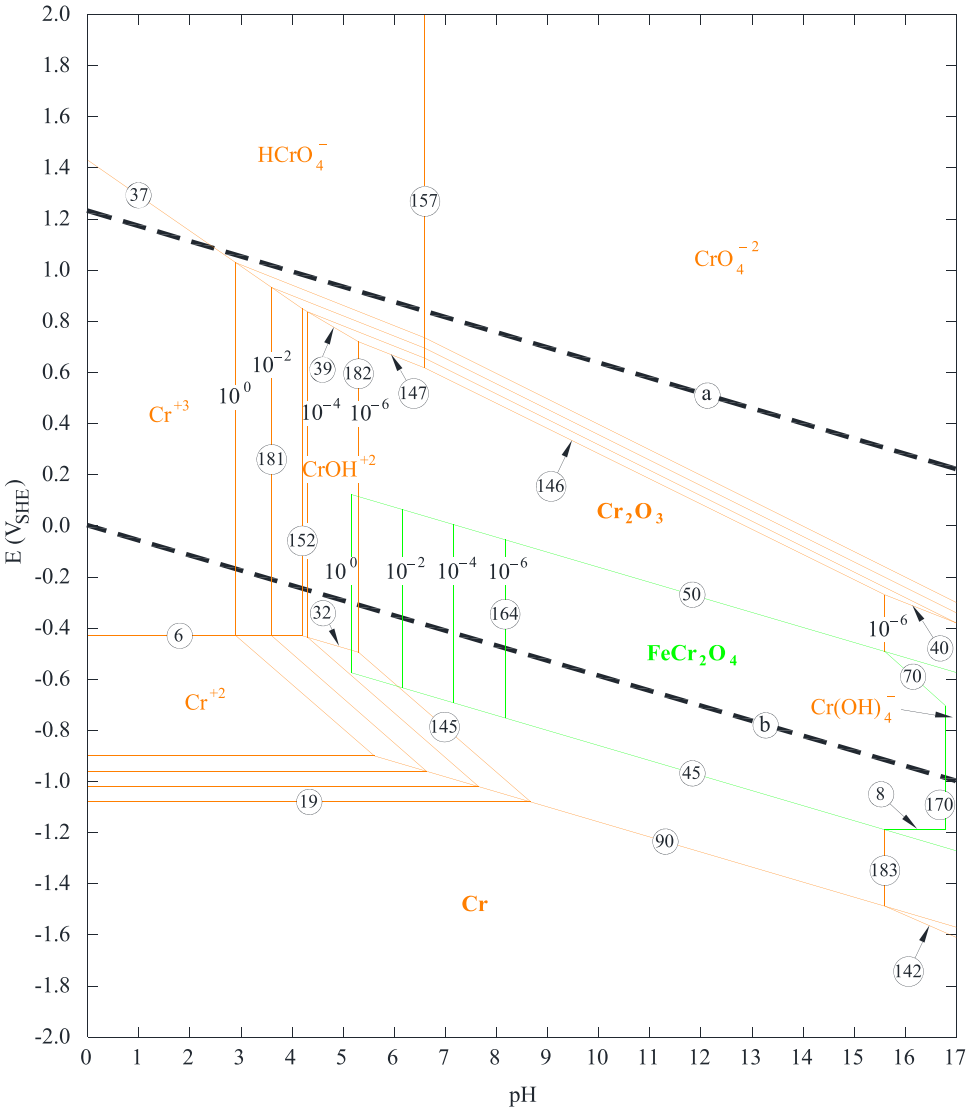

Fig. 9. Pourbaix diagram involving chromium species for Fe-Cr alloys in LiBr/H_2O solution of 850 g/L.

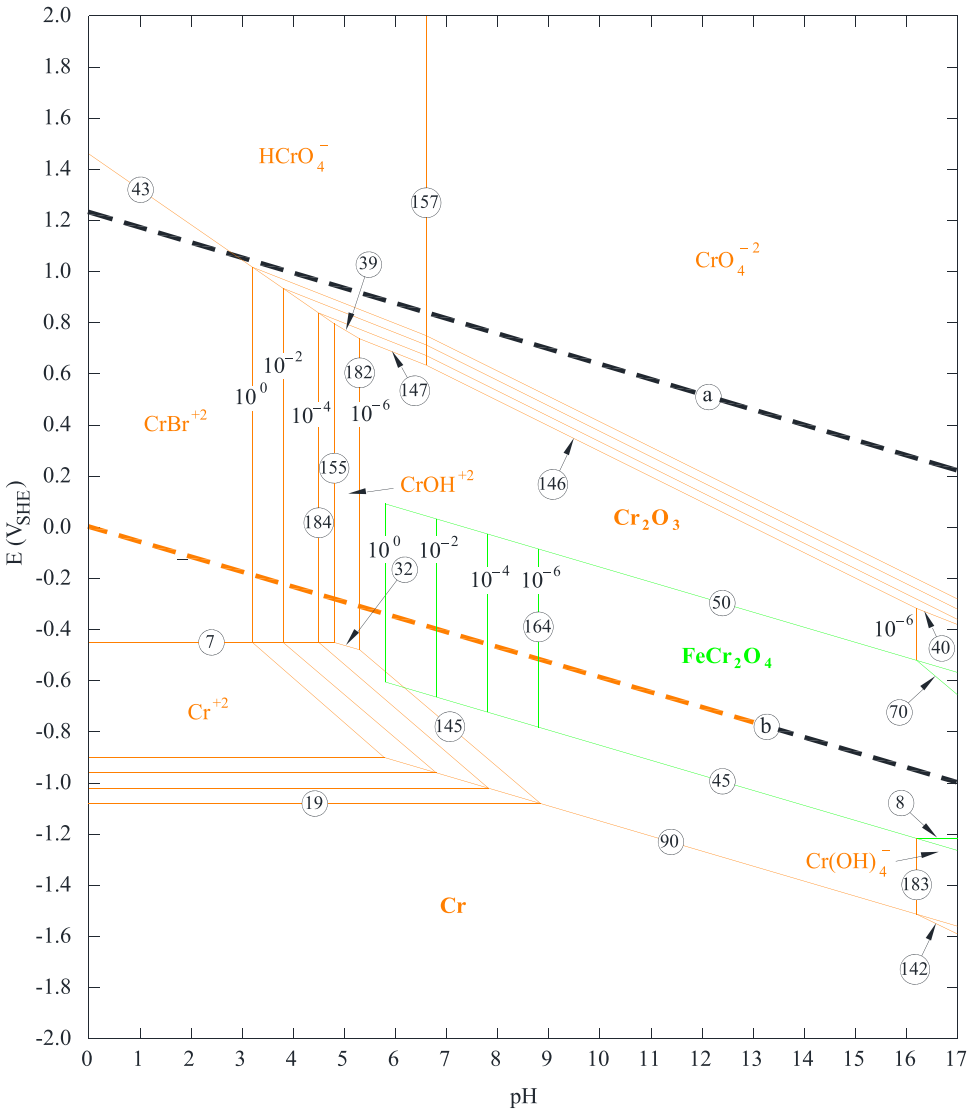

Fig. 10. Pourbaix diagram involving chromium species for Fe-Cr alloys in LiBr/H_2O solution of 992 g/L.

3.3. Simplified Pourbaix diagrams for Fe-Cr alloys in LiBr absorption machines

Figs. 11 and 12 show the influence of LiBr concentration on the simplified Pourbaix diagrams for Fe-Cr alloys, considering the stable iron-chromium species together with stable iron species (Fig. 11) and stable chromium species (Fig. 12). For the representation of the diagrams, the aqueous species' activity is considered to be 10^{-6}. In these types of diagrams, the stable species' corrosion and alkaline corrosion regions are illustrated by shaded areas, which distinguish them from the immunity and passivation regions.

In reference to the stable iron species (Fig. 11), it should be indicated that the higher the LiBr concentration, the larger the corresponding corrosion region for the aqueous iron species at acid and neutral pH. The alkaline corrosion region of aqueous iron species deviates to higher pHs when LiBr concentration increases, and that region disappears in the LiBr/H_2O solutions of 700, 850 and 992 g/L (Figs. 11c, 11d and 11e, respectively). The size of the immunity region of iron, the passivation region of solid iron and iron-chromium species, and the corrosion region of aqueous iron species at high potentials all decrease when LiBr concentration is increased.

Regarding the stable chromium species (Fig. 12), it should be noted that the dimensions of the corrosion region at acid and neutral pH of aqueous chromium species increase when LiBr concentration is increased. The alkaline corrosion region of aqueous chromium species shifts to higher pHs when LiBr concentration is increased. The extent of the immunity region of chromium, the passivation region of solid chromium and iron-chromium species, and the corrosion region of aqueous chromium species at high potential values decrease slightly when LiBr concentration is increased.

4. Conclusions

From the Pourbaix diagrams for Fe-Cr alloys in the absence of and in the presence of aqueous solutions with high concentrations of LiBr, the following conclusions can be drawn:

- Based on the Pourbaix diagrams in the absence of LiBr, a corrosion region is formed from acid to neutral pH by the aqueous species Fe^{+2}, Fe^{+3}, Cr^{+2}, Cr^{+3} and $CrOH^{+2}$.
- Based on the Pourbaix diagrams in the presence of LiBr, $FeBr_2$(aq), $FeBr_3$(aq), Cr^{+2}, Cr^{+3} and $CrOH^{+2}$ are the stable aqueous species in the corrosion region at acid and neutral pH for LiBr/H_2O solutions with concentrations of 400, 700 and 850 g/L, while $CrBr^{+2}$ replaces Cr^{+3} at the concentration of 992 g/L. The higher the LiBr concentration, the larger the dimensions of the corrosion region.

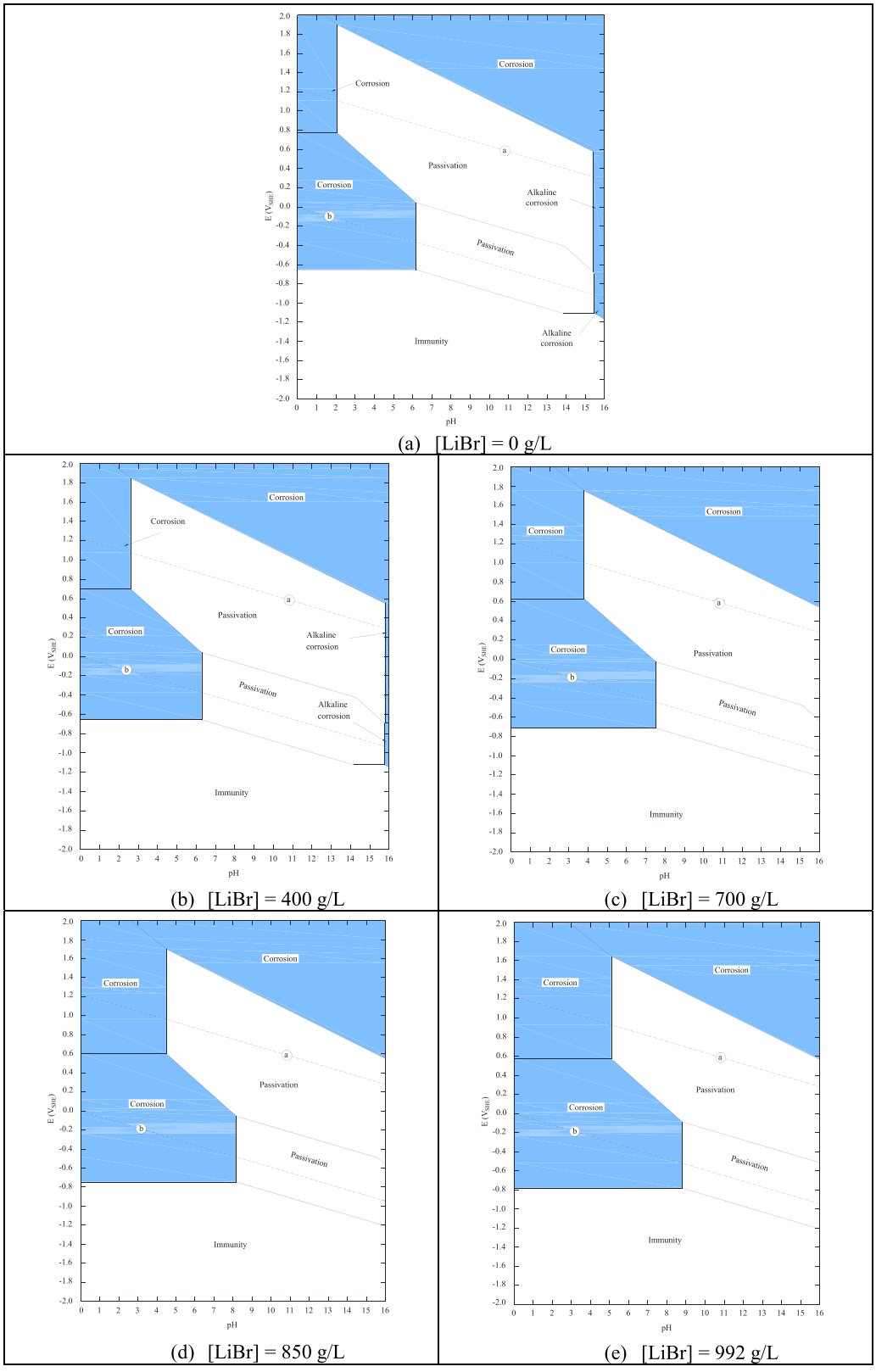

Fig.11. Simplified Pourbaix diagram involving iron species for Fe-Cr alloys (a) in the absence of and in the presence of $LiBr/H_2O$ solutions of (b) 400 g/L, (c) 700 g/L, (d) 850 g/L and (e) 992 g/L, at an activity value of 10^{-6} for the aqueous iron species.

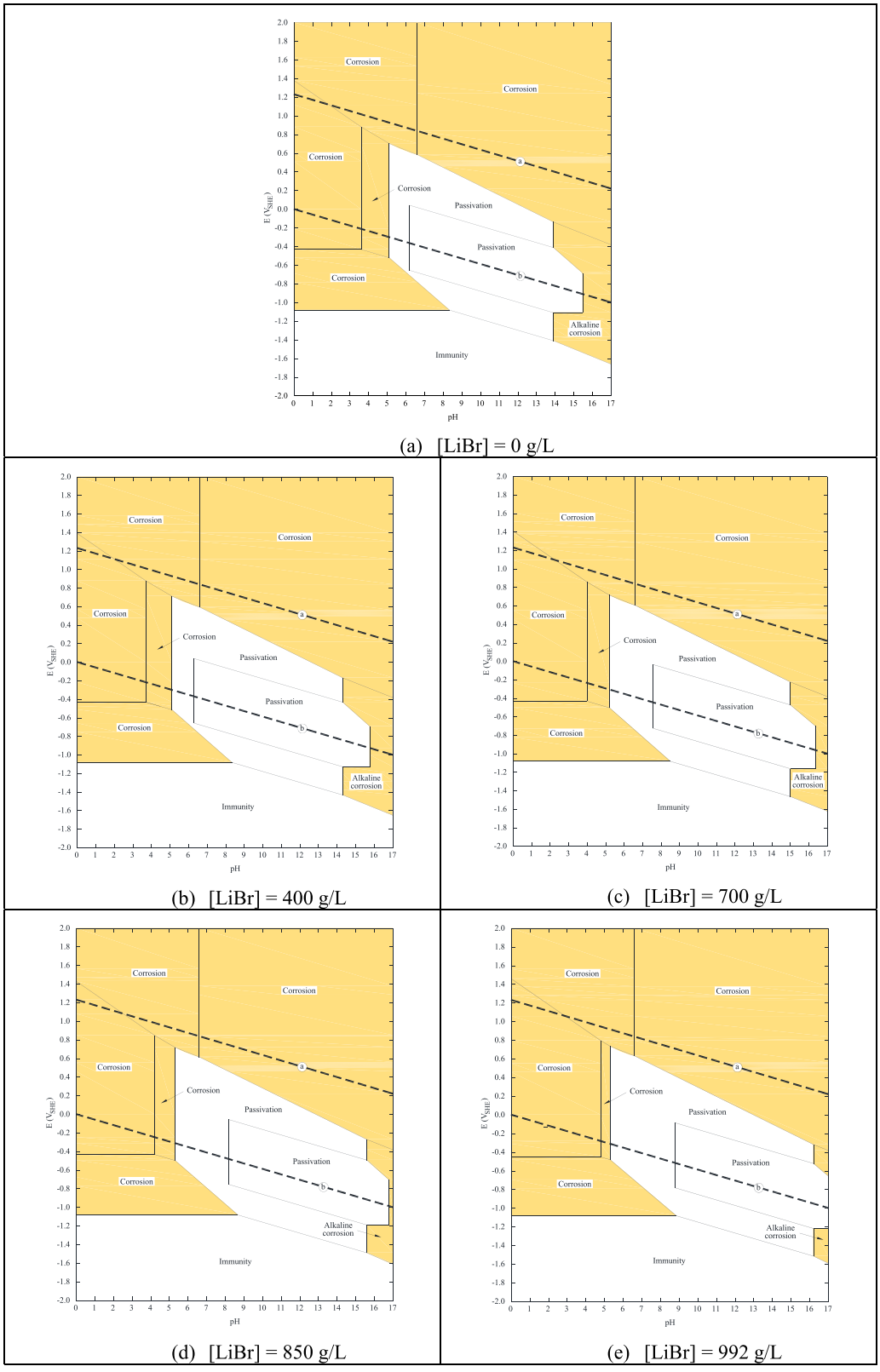

Fig. 12. Simplified Pourbaix diagram involving chromium species for Fe-Cr (a) in the absence of and in the presence of LiBr/H_2O solutions of (b) 400 g/L, (c) 700 g/L, (d) 850 g/L and (e) 992 g/L, at an activity value of 10^{-6} for the aqueous chromium species.

- The formation of the solid iron-chromium species $FeCr_2O_4$ in the Pourbaix diagrams for Fe-Cr alloys destabilises the solid iron species $Fe(OH)_2$ and Fe_3O_4, which appeared in the Pourbaix diagrams for Fe both in the absence of and in the presence of LiBr. $FeCr_2O_4$ forms a new passivation zone inside the stability zone of the solid species Cr_2O_3, which reaches higher pH values and partially occupies the alkaline corrosion zone of the aqueous species $Cr(OH)_4^-$.
- Regarding the influence of LiBr concentration, the immunity region of Fe and Cr and the passivation region of solid species $FeCr_2O_4$, Fe_2O_3 and Cr_2O_3 decrease when LiBr concentration increases. The alkaline corrosion region of aqueous species $Fe(OH)_4^{-2}$, $Fe(OH)_4^-$ and $Cr(OH)_4^-$ shifts to higher pHs as LiBr concentration increases. The corrosion region of aqueous species FeO_4^{-2}, $HCrO_4^-$ and CrO_4^{-2} at high potential values decreases when LiBr concentration is increased.
- In relation to the effect of the activity value of the aqueous species, the corrosion region at acid and neutral pH and the corrosion region at high potential values decrease when activity value is increased. The alkaline corrosion region shifts to higher pH values by increasing activity value. Consequently, the immunity region and the passivation region increase with an increase in the activity value.

The Pourbaix diagrams developed in this work are not only of scientific interest but also can be used in refrigeration systems to predict the corrosion of stainless steel in the aggressive conditions found in LiBr absorption machines. A productive path for future research could be the development of the Pourbaix diagrams for iron-chromium-nickel or iron-chromium-nickel-molybdenum alloys in aqueous concentrated LiBr solutions. These have not yet been studied, and they would make it possible to predict the corrosion behaviour of these highly alloyed stainless steels in the environment found inside LiBr absorption machines.

CRediT authorship contribution statement

M.J. Muñoz-Portero: Writing – original draft, Visualization, Methodology, Investigation, Formal analysis, Conceptualization. **T. Nachiondo:** Writing – review & editing, Software, Methodology. **J. García-Antón:** Writing – review & editing, Supervision, Conceptualization.

Declaration of competing interest

The authors declare that they have no known competing financial interests or personal relationships that could have appeared to influence the work reported in this paper.

Data availability

Data will be made available on request.

Acknowledgements

The authors acknowledge “Idiomas Complutense - Gabinete Lingüístico” at the Complutense University of Madrid for its language assistance. Funding for open access charge: CRUE-Universitat Politècnica de València.

References

[1] H.Z. Sharif, A.M. Leman, S. Muthuraman, M.N.M. Salleh, S. Zakaria, Performance analysis of single stage LiBr-water absorption machine operated by waste thermal energy of internal combustion engine: case study, AIP Conf. Proc. 1885 (2017) 020210, https://doi.org/10.1063/1.5002404.
[2] I.B. Butt, J. Tan, A. Waqas, M. Ali, A. Javed, A.Y. Ali, Effect of modified flow schemes of heat transfer fluid on the performance of a solar absorption-cooling system for an educational building in Pakistan, Appl. Sci. 10 (2020) 3327, https://doi.org/10.3390/app10093327.
[3] A.S. Soliman, S. Zhu, L. Xu, J. Dong, P. Cheng, Design of an H_2O-LiBr absorption system using PCMs and powered by automotive exhaust gas, Appl. Therm. Eng. 191 (2021) 116881, https://doi.org/10.1016/j.applthermaleng.2021.116881.
[4] A. Zendehnam, F. Pourfayaz, Sensitivity analysis of avoidable and unavoidable exergy destructions in a parallel double-effect LiBr-water absorption cooling system, Energy Sci. Eng. 11 (2023) 527–546, https://doi.org/10.1002/ese3.1344.
[5] K. Wang, O. Abdelaziz, P. Kisari, A. Vineyard, State-of-the-art review on crystallization control technologies for water/LiBr absorption heat pumps, Int. J. Refrig. 34 (2011) 1325–1337, https://doi.org/10.1016/j.ijrefrig.2011.04.006.
[6] B. Bakhtiari, L. Fradette, R. Legros, J. Paris, A model for analysis and design of H_2O-LiBr absorption heat pumps, Energy Convers. Manag. 52 (2011) 1439–1448, https://doi.org/10.1016/j.enconman.2010.09.037.
[7] J. Wonchala, M. Hazledine, K.G. Boulama, Solution procedure and performance evaluation for a water-LiBr absorption refrigeration machine, Energy 65 (2014) 272–284, https://doi.org/10.1016/j.energy.2013.11.087.
[8] A.A.V. Ochoa, J.C.C. Dutra, J.R.G. Henríquez, J. Rohatgi, Energetic and exergetic study of a 10RT absorption chiller integrated into a microgeneration system, Energy Convers. Manag. 88 (2014) 545–553, https://doi.org/10.1016/j.enconman.2014.08.064.
[9] B. Narváez-Romo, M. Chhay, E.W. Zavaleta-Aguilar, J.R. Simoes-Moreira, A critical review of heat and mass transfer correlations for LiBr-H_2O and NH_3-H_2O absorption refrigeration machines using falling liquid film technology, Appl. Therm. Eng. 123 (2017) 1079–1095, https://doi.org/10.1016/j.applthermaleng.2017.05.092.
[10] S.Y. Lee, S.K. Lee, J.T. Chung, Y.T. Kang, Numerical evaluation of a compact generator design for steam driven H_2O/LiBr absorption chiller application, Energy 152 (2018) 512–520, https://doi.org/10.1016/j.energy.2018.03.161.
[11] S.K. Lee, J.W. Lee, H. Lee, J.T. Chung, Y.T. Kang, Optimal design of generators for H_2O/LiBr absorption chiller with multi-heat sources, Energy 167 (2019) 47–59, https://doi.org/10.1016/j.energy.2018.10.185.
[12] K.L. Cézar, A.G.A. Caldas, A.M.A. Caldas, M.C.L. Cordeiro, C.A.C. Dos Santos, K. L. Cézar, A.A.V. Ochoa, P.S.A. Michima, Development of a novel flow control system with Arduino microcontroller embedded in double effect absorption chillers using the LiBr/H_2O pair, Int. J. Refrig. 111 (2020) 124–135, https://doi.org/10.1016/j.ijrefrig.2019.11.014.
[13] S.H. Seo, S.D. Oh, H.Y. Kwak, Thermodynamic, exergetic and thermoeconomic analyses of double-effect LiBr-water absorption refrigeration systems with a 5 kW high temperature PEMFC as heat source for data center applications, Energies 15 (2022) 3101, https://doi.org/10.3390/en15093101.
[14] A. Soliz, L. Cáceres, Corrosion behavior of carbon steel in LiBr in comparison to NaCl solutions under controlled hydrodynamic conditions, Int. J. Electrochem. Sci. 10 (2015) 5673–5693, https://doi.org/10.1016/S1452-3981(23)17286-5.
[15] A. Soliz, K.J.J. Mayrhofer, L. Cáceres, Influence of hydrodynamic flow patterns on the corrosion behavior of carbon steel in a neutral LiBr solution, Int. J. Electrochem. Sci. 13 (2018) 10050–10075, https://doi.org/10.20964/2018.11.08.
[16] Y. Cho, S. Han, H. Seo, M. Shin, S. Woo, S. Jeong, Corrosion and inhibition process of carbon steel in LiBr-H_2O solution, J. Mech. Sci. Technol. 33 (2019) 2995–3000, https://doi.org/10.1007/s12206-019-0549-x.
[17] J. Yoo, S. Han, Y. Nam, S. Jeong, Effect of shot-peening on the passive film formation and corrosion of carbon steel in LiBr aqueous solutions, J. Mech. Sci. Technol. 34 (2020) 4037–4041, https://doi.org/10.1007/s12206-020-2214-9.
[18] T. Irie, D. Morihashi, Y. Hirohata, T. Haruna, Polarization curves of carbon steel in concentrated LiBr solutions containing LiOH and Li_2MoO_4 at different temperatures after short immersion, Mater. Trans. 62 (2021) 420–426, https://doi.org/10.2320/matertrans.MT-M2020298.
[19] A.K. Larios-Galvez, R. Guardian-Tapia, R. Lopez-Sesenes, J.G. Gonzalez-Rodriguez, Corrosion behaviour of 1018 carbon steel in LiBr-H_2O-$CaCl_2$-$LiNO_3$ mixtures, Int. J. Electrochem. Sci. 17 (2022) 220131, https://doi.org/10.20964/2022.01.18.
[20] R. Sánchez-Tovar, M.T. Montañés, J. García-Antón, Thermogalvanic corrosion and galvanic effects of copper and AISI 316L stainless steel pairs in heavy LiBr brines under hydrodynamic conditions, Corros. Sci. 60 (2012) 118–128, https://doi.org/10.1016/j.corsci.2012.04.001.
[21] E. Sarmiento, J.G. González-Rodriguez, A.M. Ramirez-Arteaga, J. Uruchurtu, Corrosion inhibition of 316L stainless steel in LiBr+etileneglycol+H_2O by using inorganic inhibitors, Int. J. Electrochem. Sci. 8 (2013) 12417–12433, https://doi.org/10.1016/S1452-3981(23)13277-9.
[22] A. Goodarzi, I. Danaee, H. Eskandari, S. Nikmanesh, Electrochemical corrosion behavior of duplex stainless steel AISI 2205 in ethylene glycol-water mixture in the presence of 50 W/V% LiBr, J. Electrochem. Sci. Technol. 7 (2016) 58–67, https://doi.org/10.5229/JECST.2016.7.1.58.
[23] E.A. Abd El Meguid, S.S. Abd El Rehim, S.A. Al Kiey, Inhibitory effect of cetyltrimethyl ammonium bromide on the corrosion of 904L stainless steel in LiBr solution, Corros. Eng. Sci. Technol. 51 (2016) 429–437, https://doi.org/10.1080/1478422X.2015.1131799.
[24] S. Zolfaghari, A.R. Baboukani, A. Ashrafi, A. Saatchi, Investigation the effects of Na_2MoO_4 as an inhibitor on electrochemical corrosion behavior of 316L stainless steel in LiBr solution, Zast. Mater. 59 (2018) 108–116, https://doi.org/10.5937/ZasMat1801110Z.
[25] M.A. Kappes, Localized corrosion and stress corrosion cracking of stainless steels in halides other than chlorides solutions: a review, Corros. Rev. 38 (2020) 1–24, https://doi.org/10.1515/corrrev-2019-0061.
[26] S. Hu, R. Liu, L. Liu, Y. Cui, F. Wang, Influence of temperature and hydrostatic pressure on the galvanic corrosion between 90/10 Cu-Ni and AISI 316L stainless

steel, J. Mater. Res. Technol. 13 (2021) 1402–1415, https://doi.org/10.1016/j.jmrt.2021.05.067.
[27] C. Cuevas-Arteaga, J. Porcayo Calderón, C.F. Campos Sedano, J.A. Rodríguez, Comparison of corrosion resistance of carbon steel and some stainless steels exposed to LiBr-H_2O solution al low temperatures, Int. J. Electrochem. Sci. 7 (2012) 445–470, https://doi.org/10.1016/S1452-3981(23)13351-7.
[28] A.K. Larios-Galvez, R. Lopez-Sesenes, E. Sarmiento-Bustos, I. Rosales, J. Uruchurtu-Chavarin, J. Porcayo-Calderon, J.G. Gonzalez-Rodriguez, Corrosion behavior of steels in LiBr-H_2O-$CaCl_2$-$LiNO_3$ systems, Metals 12 (2022) 279, https://doi.org/10.3390/met12020279.
[29] B. Beverskog, I. Puigdomenech, Revised Pourbaix diagrams for iron at 25-300 ºC, Corros. Sci. 38 (1996) 2121–2135, https://doi.org/10.1016/S0010-938X(96)00067-4.
[30] B. Beverskog, I. Puigdomenech, Pourbaix diagrams for the ternary system of iron-chromium-nickel, Corrosion 55 (1999) 1077–1087, https://doi.org/10.5006/1.3283945.
[31] T. Nishimura, T. Kodama, Clarification of chemical state for alloying elements in iron rust using a binary-phase potential-pH diagram and physical analyses, Corros. Sci. 45 (2003) 1073–1084, https://doi.org/10.1016/S0010-938X(02)00186-5.
[32] W.G. Cook, R.P. Olive, Pourbaix diagrams for the iron-water system extended to high-subcritical and low-supercritical conditions, Corros. Sci. 55 (2012) 326–331, https://doi.org/10.1016/j.corsci.2011.10.034.
[33] L.L. Pesterfield, J.B. Maddox, M.S. Crocker, G.K. Schweitzer, Pourbaix (E-pH-M) diagrams in three dimensions, J. Chem. Educ. 89 (2012) 891–899, https://doi.org/10.1021/ed200423n.
[34] Y. Baoju, Z. Zhigang, W. Xiaoyuan, Y. Xuebo, C. Shuai, Pourbaix diagrams to decipher precipitation conditions of Si-Fe-Mn-oxyhydroxides at the PACMANUS hydrothermal field, Acta Oceanol. Sin. 33 (2014) 58–66, https://doi.org/10.1007/s13131-014-0572-9.
[35] Z. Zeng, M.K.Y. Chan, Z.J. Zhao, J. Kubal, D. Fan, J. Greeley, Towards first principles-based prediction of highly accurate electrochemical Pourbaix diagrams, J. Phys. Chem. C 119 (2015) 18177–18187, https://doi.org/10.1021/acs.jpcc.5b03169.
[36] A.G. Tyurin, D.A. Manannikov, V.P. Parshukov, A.V. Antonova, P.A. Nikolaychuk, Method of estimation of corrosion stability of multicomponent alloys using equilibrium and polarization potential-pH diagrams, Anti-Corros. Method. M. 63 (2016) 386–397, https://doi.org/10.1108/ACMM-12-2014-1479.
[37] E. Protopopoff, P. Marcus, Potential-pH diagrams for Ni-Cr-Fe alloys and Pb adsorption on Ni-Cr-Fe alloys surfaces in water at 25 ºC and high temperature (250-350 ºC), J. Electrochem. Soc. 165 (2018) C433–C440, https://doi.org/10.1149/2.1291807jes.
[38] S.C. Perry, S.M. Gateman, L.I. Stephens, R. Lacasse, R. Schulz, J. Mauzeroll, Pourbaix diagrams as a simple route to first principles corrosion simulation, J. Electrochem. Soc. 166 (2019) C3186–C3192, https://doi.org/10.1149/2.0111911jes.
[39] J. Fu, X. Jiang, W. Han, Z. Cao, Enhancing the cycling stability of transition-metal-oxide-based electrochemical electrode via Pourbaix diagram engineering, Energy Stor. Mater. 42 (2021) 252–258, https://doi.org/10.1016/j.ensm.2021.07.037.
[40] S.H. Drissi, Ph. Refait, M. Abdelmoula, J.M.R. Génin, The preparation and thermodynamic properties of Fe (II)-Fe(III) hydroxide-carbonate (green rust 1); Pourbaix diagram of iron in carbonate-containing aqueous media, Corros. Sci. 37 (1995) 2025–2041, https://doi.org/10.1016/0010-938X(95)00096-3.
[41] I. Azoulay, C. Rémazeilles, Ph. Refait, Determination of standard Gibbs free energy of formation of chukanovite and Pourbaix diagrams of iron in carbonated media, Corros. Sci. 58 (2012) 229–236, https://doi.org/10.1016/j.corsci.2012.01.033.
[42] X. Zhou, C. Liao, Y. Wang, Y. Zhu, Constructing the Pourbaix diagram of Fe-Cl^--H_2O ternary system under supercritical water conditions, Electrochim. Acta 377 (2021) 138075, https://doi.org/10.1016/j.electacta.2021.138075.
[43] Y. Zhao, J. Xie, G. Zeng, T. Zhang, D. Xu, F. Wang, Pourbaix diagram for HP-13Cr stainless steel in the aggressive oilfield environment characterized by high temperature, high CO_2 partial pressure and high salinity, Electrochim. Acta 293 (2019) 116–127, https://doi.org/10.1016/j.electacta.2018.08.156.
[44] M.J. Muñoz-Portero, J. García-Antón, J.L. Guiñón, V. Pérez-Herranz, Pourbaix diagrams for copper in aqueous lithium bromide concentrated solutions, Corrosion 60 (2004) 749–756, https://doi.org/10.5006/1.3287854.
[45] M.J. Muñoz-Portero, J. García-Antón, J.L. Guiñón, V. Pérez-Herranz, Pourbaix diagrams for nickel in concentrated aqueous lithium bromide solutions at 25 ºC, Corrosion 63 (2007) 625–634, https://doi.org/10.5006/1.3278412.
[46] M.J. Muñoz-Portero, J. García-Antón, J.L. Guiñón, V. Pérez-Herranz, Pourbaix diagrams for chromium in concentrated aqueous lithium bromide solutions at 25 ºC, Corros. Sci. 51 (2009) 807–819, https://doi.org/10.1016/j.corsci.2009.01.004.
[47] M.J. Muñoz-Portero, J. García-Antón, J.L. Guiñón, R. Leiva-García, Pourbaix diagrams for titanium in concentrated aqueous lithium bromide solutions at 25 ºC, Corros. Sci. 53 (2011) 1440–1450, https://doi.org/10.1016/j.corsci.2011.01.013.
[48] M.J. Muñoz-Portero, T. Nachiondo, E. Blasco-Tamarit, A. Vicent-Blesa, J. García-Antón, Potential-pH diagrams of iron in concentrated aqueous LiBr solutions at 25 ºC, Corrosion 74 (2018) 1102–1116, https://doi.org/10.5006/2865.
[49] A.J. Bard, R. Parsons, J. Jordan, Standard Potentials in Aqueous Solution, Marcel Dekker, New York, 1985.
[50] J. Rumble, CRC Handbook of Chemistry and Physics, 98th ed., CRC Press, Boca Raton, 2017.
[51] B. Beverskog, I. Puigdomenech, Revised Pourbaix diagrams for chromium at 25-300 ºC, Corros. Sci. 39 (1997) 43–57, https://doi.org/10.1016/S0010-938X(97)89244-X.
[52] M. Pourbaix, Atlas of Electrochemical Equilibria in Aqueous Solutions, 1st ed., Pergamon Press, New York, 1966.
[53] C.L. Kusik, H.P. Meissner, Electrolyte activity coefficients in inorganic processing, AIChE Symp. Ser. 74 (1978) 14–20.
[54] H.P. Meissner, Prediction of activity coefficients of strong electrolytes in aqueous systems, ACS Symp. Ser. 133 (1980) 495–511.
[55] C.L. Kusik, H.P. Meissner, Vapor pressures of water over aqueous solutions of strong electrolytes, Ind. Eng. Chem. Process Des. Dev. 12 (1973) 112–115.
[56] M.J. Muñoz-Portero, T. Nachiondo, Development of a software application for the construction of the simplified pourbaix diagrams used in the study of the corrosion, in: L.G. Chova, A.L. Martínez, I.C. Torres (Eds.), 7th International Technology, Education, and Development Conference (INTED 2013), IATED-Int. Assoc, Technology Education & Development, Valencia, 2013, pp. 5978–5986.